Paleoceanography and Paleoclimatology

RESEARCH ARTICLE
10.1029/2024PA004894

Two-Stage Climate and Vegetation Change at the East Asian Monsoonal Margin Across the Miocene Climatic Optimum

Jian Wang[1,2], Xinying Zhou[2,3], Shiqi Wang[2], Jie Ye[2], Junchi Liu[2], Yan Zheng[2], Thomas A. Stidham[2,3], Keliang Zhao[2], Hermann Behling[4], and Xiaoqiang Li[2,3]

[1]Department of Archaeology and Anthropology, University of Chinese Academy of Sciences, Beijing, China, [2]Key Laboratory of Vertebrate Evolution and Human Origins, Institute of Vertebrate Paleontology and Paleoanthropology, Chinese Academy of Sciences, Beijing, China, [3]College of Earth and Planetary Sciences, University of Chinese Academy of Sciences, Beijing, China, [4]Department of Palynology and Climate Dynamics, University of Göttingen, Göttingen, Germany

Abstract The change in vegetation at the margins of the East Asian summer monsoon (EASM) during the Miocene Climatic Optimum (MCO) remains poorly understood. Here, we present a high-resolution terrestrial sequence, paleomagnetically dated to 18.2–13.5 Ma, from the Tongxin Basin of midwestern China. Our multi-indicator analysis, encompassing pollen, $\delta^{13}C_{TOC}$, $\delta^{18}O_{carb}$-$\delta^{13}C_{carb,}$ and magnetic susceptibility, reveals that the regional vegetation and climate had two distinct stages during the MCO, manifesting as stable arid steppe from 17.0 to 16.0 Ma, and woodland steppe with six forested environments from 16.0 to 14.0 Ma. Together with other adjacent records, this supports the EASM as the main control on terrestrial vegetation. Further comparisons of marine-terrestrial data and time series analysis suggest that in the late MCO, the oceanic carbon reservoir (OCR) experienced strong perturbations (mainly C_{max} events) accompanied by multiple oscillations. The instability signals likely impacted and were amplified as rapid shifts in forest-steppe environments at the monsoon margins via EASM. Our study highlights the regulation of inland ecologically vulnerable areas by low-latitude forcing in a greenhouse world.

Plain Language Summary Exploring the response of vegetation to the Miocene Climatic Optimum (MCO, ~17.0–14.0 Ma) can serve as an analogy for studies of ecological impacts under future global warming. Here, we perform magnetostratigraphic dating and past vegetation-climate reconstruction in high-resolution terrestrial sediments in the Tongxin Basin of Midwest China, a region sensitive to the East Asian summer monsoon (EASM). The records of several indicators, including pollen, $\delta^{13}C_{TOC}$, $\delta^{18}O_{carb}$-$\delta^{13}C_{carb}$ and magnetic susceptibility, indicate that the regional climate and vegetation changed in two major stages across the warm MCO. Between 16.0 and 17.0 Ma, the regional vegetation was predominantly stable arid steppe, followed by at least six rapid oscillations between arid steppe and forest environments between 14.0 and 16.0 Ma. Further analyses show that EASM intensity dominates regional changes in vegetation, and its changing pattern is quasi-similar to global oceanic $\delta^{13}C$ changes reflecting the state of oceanic carbon reservoir (OCR). Multiple rapid shifts in the forest-steppe landscape during the late MCO are closely related to fluctuations in the EASM system, which are modulated by strong oscillations in the OCR. Our study reveals the non-negligible role of the low-latitude marine carbon cycle in forcing inland ecologically vulnerable areas during global climatic warming.

Key Points:

- The age of the Miocene Tongxin Fauna is constrained to 18.0–14.0 Ma by magnetostratigraphy and biostratigraphy
- The stability of the regional climate-vegetation system underwent a two-stage evolutionary pattern during the Miocene Climatic Optimum (MCO)
- Regional vegetation oscillations are likely to respond to ocean carbon reservoir perturbation in the late MCO

Supporting Information:

Supporting Information may be found in the online version of this article.

Correspondence to:

X. Zhou and X. Li,
zhouxinying@ivpp.ac.cn;
lixiaoqiang@ivpp.ac.cn

Citation:

Wang, J., Zhou, X., Wang, S., Ye, J., Liu, J., Zheng, Y., et al. (2024). Two-stage climate and vegetation change at the East Asian monsoonal margin across the Miocene Climatic Optimum. *Paleoceanography and Paleoclimatology*, *39*, e2024PA004894. https://doi.org/10.1029/2024PA004894

Received 24 MAR 2024
Accepted 5 AUG 2024

Author Contributions:

Conceptualization: Jian Wang, Xinying Zhou, Xiaoqiang Li
Data curation: Junchi Liu, Yan Zheng, Hermann Behling
Formal analysis: Jian Wang, Xinying Zhou, Shiqi Wang, Junchi Liu, Yan Zheng, Keliang Zhao, Hermann Behling
Funding acquisition: Jian Wang, Xinying Zhou, Xiaoqiang Li
Investigation: Jian Wang, Shiqi Wang, Jie Ye
Methodology: Jian Wang
Resources: Jian Wang
Software: Jian Wang
Supervision: Xinying Zhou, Xiaoqiang Li
Writing – original draft: Jian Wang
Writing – review & editing: Jian Wang, Xinying Zhou, Thomas A. Stidham, Xiaoqiang Li

1. Introduction

The Miocene Climatic Optimum (MCO), occurring ~17.0–~14.0 Ma million years ago (Ma), represents a globally warm time interval punctuating the long-term Cenozoic cooling trend (Zachos et al., 2008). This period is increasingly regarded as a good analog for future climate scenarios, because of 7.6 ± 2.3°C temperature increases and near-future CO_2 concentrations (pCO_2) of ~450–600 ppm (Rae et al., 2021; Steinthorsdottir, Jardine, & Rember, 2021). A striking feature of the MCO was the reduced Antarctic ice-sheet that is thought to have accompanied the warming (Shevenell et al., 2004; Warny et al., 2009; Wubben et al., 2023), implying that high-latitude forcing was much less of a climate driver than during the Quaternary. Although the forcing underlying the MCO remains enigmatic, growing evidence hints at an important role for the low-latitude ocean carbon reservoir (OCR) (Holbourn et al., 2022). Deep-sea benthic isotope and $CaCO_3$ records reveal prominent 100 kyr variability with 400 kyr cyclicity through the MCO, pointing to a tight coupling between the OCR and climate variations (Holbourn et al., 2015; Wang et al., 2019). The climate experienced multiple oscillations linked to the OCR during the late MCO, manifested by high-amplitude climate variations and intense perturbations of the carbon

cycle in the eastern Pacific (Holbourn et al., 2013). Globally, the most compelling story of the OCR is the six carbon isotope maxima (C_{max}/CM) events with >1‰ $\delta^{13}C$ shifts (Diester-Haass et al., 2013; Sosdian et al., 2020), representing the capability of the carbon cycle to regulate climate evolution.

The monsoon circulation system links terrestrial vegetation ecosystems and the ocean carbon cycle. Driven by the land-ocean thermal gradient and cross-equatorial pressure gradient over the Asian-Pacific region (Ding & Chan, 2005; Geen et al., 2020), the East Asian summer monsoon (EASM) plays an important role in the evolution of forest-steppe ecotones. Due to the high sensitivity of mid-latitude terrestrial climate to oceanic changes during the MCO (Methner et al., 2020), fluctuation in EASM precipitation is capable of forcing cyclic changes in vegetation in certain areas (Zhao et al., 2020; Zhou et al., 2023). As the EASM intensified and advanced more than 10° to the west during the MCO (Miao et al., 2023), the semi-arid region experienced synchronous climatic warming and vegetation greening (Miao et al., 2012; Wang et al., 2023). However, given the paucity of continuous sedimentary sequences, the response pattern of vegetation to MCO at the EASM margins and its link to oceanic variability is poorly understood.

The Tongxin Basin not only preserves the continuous fluvial-lacustrine deposits rich in mammalian fossils, but is also sensitive to climate change as located in the forest-steppe transition zone. To reveal the history of the vegetation changes and its possible linkages with OCR across the MCO, we herein selected the Huangjiashui (HJS) section close to the monsoonal margins, and conducted detailed vegetation-climate reconstructions using multiple indicators, including pollen, total organic matter carbon isotopes ($\delta^{13}C_{TOC}$), carbonate carbon-oxygen isotopes ($\delta^{18}O_{carb}$-$\delta^{13}C_{carb}$) and magnetic susceptibility (MS). On this basis, the pattern of regional vegetation response to MCO warming is described. The possible dynamical mechanisms that trigger the response were explored by comparing with marine-terrestrial records.

2. Materials and Methods

The Tongxin Basin generally experiences a temperate monsoon-continental transitional climate zone (Figure 1). More than 60% of the limited annual precipitation (almost monsoon) is concentrated in summer, resulting in a predominance of arid steppe landscapes within the basin (Text S1 in Supporting Information S1). Additionally, the region lies downstream of the northern branch of the westerlies jet, which, in conjunction with the EASM, influences winter and spring precipitation (Curio et al., 2015). Geotectonically, the study area extends from the leading edge of the Tibetan plate extrusion and expansion to the north-east (Shi et al., 2015), where the Eocene Sikouzi Formation, Late Oligocene-Early Miocene Qingshuiying Formation, Miocene Zhang'enbao Formation, and Late Miocene-Quaternary Ganhegou Formation were deposited in sequence (Liang et al., 2021; X. Liu, Hu, et al., 2019; X. Liu, Shi, et al., 2019). Among them, the Tongxin Fauna is distributed in the sedimentary units of the Zhang'enbao Formation, and abundant mammalian fossils such as species of Artiodactyla and Proboscidea have been reported (Wang, Deng, et al., 2016; Wang, Zong, et al., 2016). Notably, the extinct ape genus *Plio-pithecus*, a group that inhabited Asia and Europe during the Miocene, has been found in this sedimentary interval (Harrison et al., 1991; Qiu & Guan, 1986).

The HJS section is an important source of representative mammalian fossils from the middle Miocene. No obvious sedimentary unconformities or hiatuses were observed in the 181m-thick section, except for the base and top of the section, which are disconformities with the suspected Sikouzi Formation and overlying Ganhegou Formation respectively (Wang, Zong, et al., 2016). The entire section belongs to the Zhang'enbao Formation, consisting of five sets of thickly bedded alternating mudstone-sandstone layers (AMSL). The light reddish-brown mudstones are generally homogeneous in texture, with occasional micro-horizontal laminations representing proximal deposition on the floodplain/lakefront. The grayish fine- and medium-grained sandstone are interpreted as typical fluvial deposits. Overall, the sedimentary facies in the HJS section alternate between fluvial stages and floodplain-lakeshore environments.

We collected ~270 paleoenvironmental samples at 0.5 m intervals from mudstone to 2.0 m intervals from sandstone for pollen and geochemical analysis. MS was measured at 0.05 m intervals and paleomagnetic dating was performed on ~500 mudstone samples using thermal demagnetization. Through pollen analysis of 110 samples (39 valid data), MS measurements of 3,621 samples, and $\delta^{13}C_{TOC}$-$\delta^{18}O_{carb}$-$\delta^{13}C_{carb}$ analysis of 169 samples (79 and 144 valid data, respectively), we conducted detailed climate-vegetation reconstruction. Acycle software was used for time series analysis of data in this study (Li et al., 2019). More information on geologic

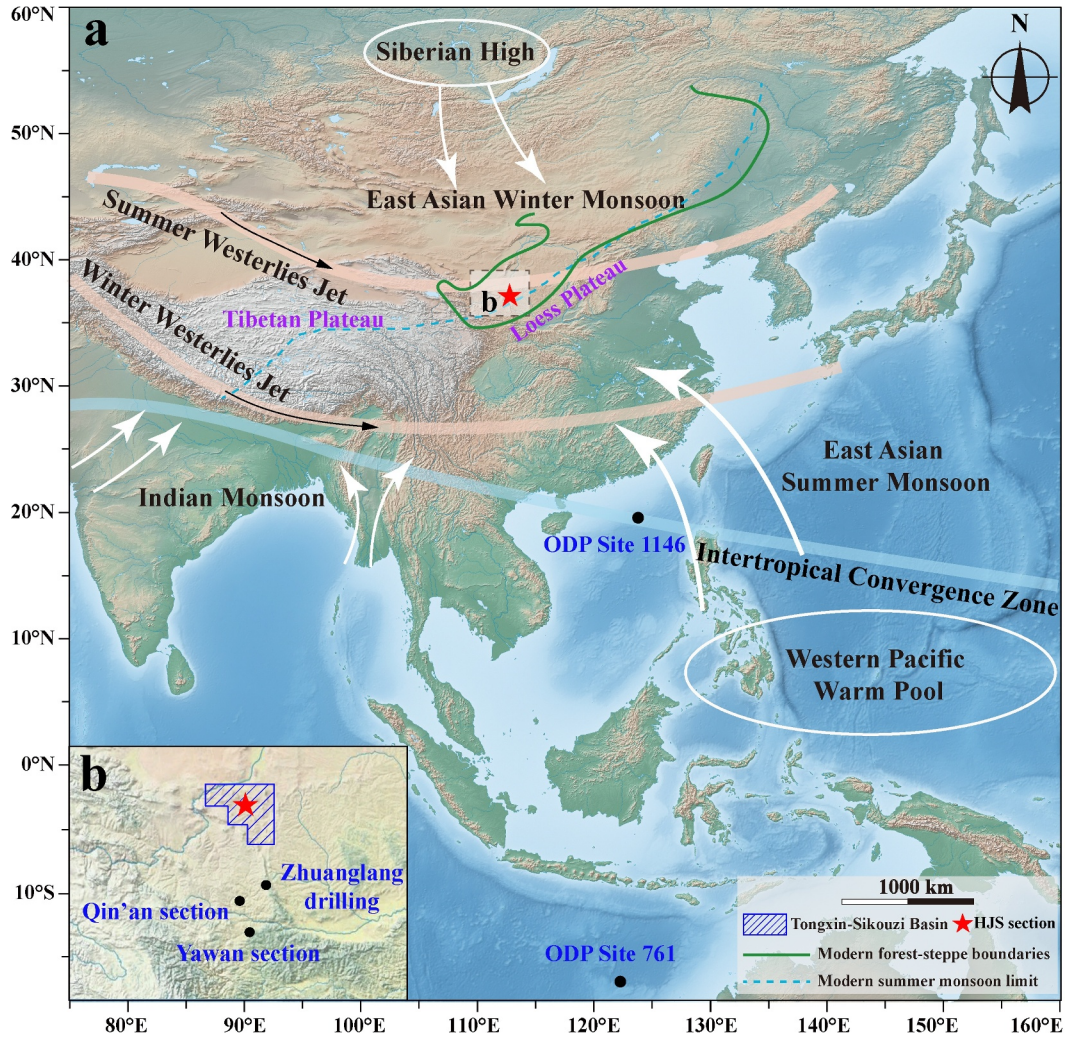

Figure 1. Atmospheric circulation patterns of the study area and the sites involved in this study. Modern forest-steppe and East Asian summer monsoon (EASM) boundaries refer to studies (Chen et al., 2019; Su et al., 2020). The general outline of the Tongxin-Shikouzi Basin in Fig. b is referenced by Wang et al. (2011). The precipitation in the study area primarily comes from the EASM, and its annual scale behavior is mainly controlled by the oscillation of the Intertropical Convergence Zone. EASM system's water, heat, and power originate from the West Pacific Warm Pool, the largest warm water region and the "heart of the climate" in the global ocean (Jian et al., 2022). The study area is often influenced by the westerly circulation (pink bands, seasonal variations in its intensity and location) and the East Asian winter monsoon associated with the Siberian High during the winter and spring seasons (Lin et al., 2024).

setting, stratigraphic sedimentation and methods are provided in Text S2 and Figures S1–S3 in Supporting Information S1.

3. Results and Discussion

3.1. Chronological Framework of the HJS Section

The continuous refinement of biostratigraphy within the Tongxin Basin has provided good constraints for alignment with paleomagnetic results. The transition between sandstone and mudstone strata is continuous throughout most of the section, with no apparent depositional interruptions, as demonstrated by the mammalian fossils. The only ambiguity involves the nearly 10 m-thick red gypsum sandstone at the top of the profile, whose drape-like deposition may be related to later aeolian accumulation. This part will not be further discussed in our study. Regional biostratigraphic studies conducted by Wang, Zong, et al. (2016) show that the Yinziling Fauna in the lower part of the Zhang'enbao Formation within the Dingjiaergou area, represented by the *Alloptox gobiensis*-

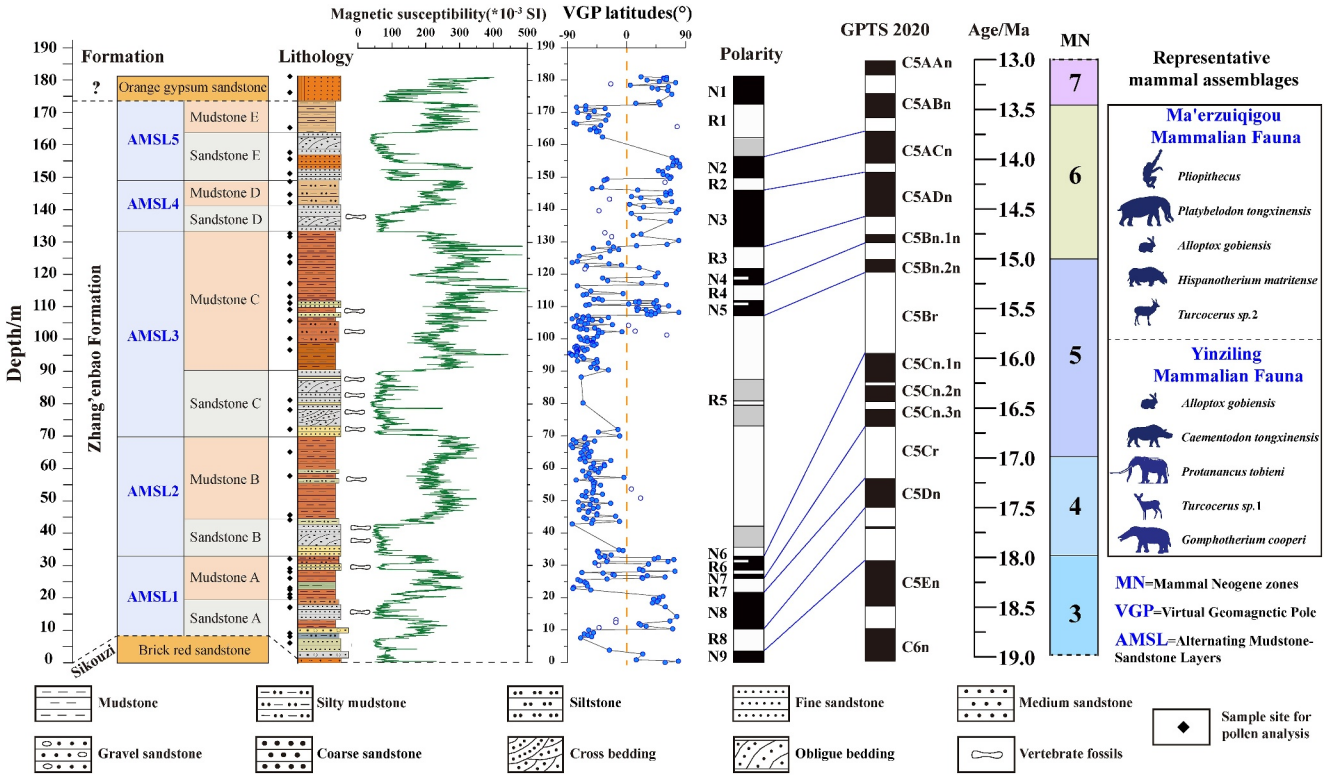

Figure 2. Lithostratigraphy, biostratigraphy, MS record and magnetostratigraphy of the HJS sequence, alongside its correlation with the GPTS2020. Polarity period is defined as the occurrence of three or more consecutive data points exhibiting the same geomagnetic polarity. Hollow dots represent data points that do not constitute a reliable polarity period. GPTS=Global Polarity Time Scale. VGP=Virtual Geomagnetic Pole.

Caementodon tongxinensis-Protanancus tobieni-Turcocerus sp.1 assemblage, corresponds to the European Mammal Neogene zone (MN) five or the late Shanwang stage of Chinese Neogene stages. The Maerzuizigou fauna in the upper middle part, marked by the *Platybelodon tongxinensis-Alloptox gobiensis-Hispanotherium matritense-Turcocerus* sp.2 assemblages, aligns with MN6 or the early Tungurian (Wang, Deng, et al., 2016; Wang, Zong, et al., 2016). Regional stratigraphic comparisons support that the HJS AMSL1 is analogous to the Yinziling Fauna of the Yinziling-Maerzuizigou section and the Gaolingzi Fauna of the Jinggou section (Figure S4 in Supporting Information S1; Table S1 in Supporting Information S1). AMSL2 in the HJS section corresponds to the second set of sandstones extending upward from the bottom of the Yinziling-Maerzuizigou section, likely corresponding to the lower part of the Mazhouzigou Fauna. AMSL3 in the HJS section parallels the Maerzuizigou Fauna in the Yinziling-Maerzuizigou section. Biochronology comparison with European Neogene mammals shows that AMSL1 in the HJS section is contemporaneous with MN5 (17.0–15.0 Ma), and AMSL3 is approximately 15.0–13.5 Ma equivalent to MN6.

The polarity sequence of the HJS section is compared with the GPTS2020 and constrained by biostratigraphy (Figure 2). *Gomphotherium cooperi*, the most primitive Gomphothere in China to date, was found at the base of the Zhang'enbao Formation. Its age range has been determined to be approximately between 18 and 19 Ma based on morphological comparisons (Li et al., 2022), implying that the age of the base of the HJS section is older than 18 Ma. The recently discovered *Percrocuta xixiaensis* sp. nov. supports an age assignment of MN5 for the middle and lower strata of the Zhang'enbao Formation of Tongxin, corresponding to the early Middle Miocene (Xiong, 2022). This evidence enables the correlation of the normal polarity N6-7 segment to correspond only to a mixed normal polarity consisting of C5Cn.1n-C5Cn.3n, while N8 and N9 are aligned sequentially with the normal polarity C5Dn and C5En, respectively. A prominent feature of the HJS polarity sequence is the extended interval of reversed polarity spanning from 110 to 40 m. Given the absence of stratigraphic gaps, this extensive reversed polarity, R5, could be matched with correspond to C5Br, representing the most prolonged reversed polarity interval between 20 and 10 Ma in GPTS2020 (Ogg, 2020). AMSL3, bearing fossils indicative of MN6 stage (15.0–13.5 Ma), combined with a dominantly normal polarity from 155 to 125 m, suggests that the intervals N5 and N4

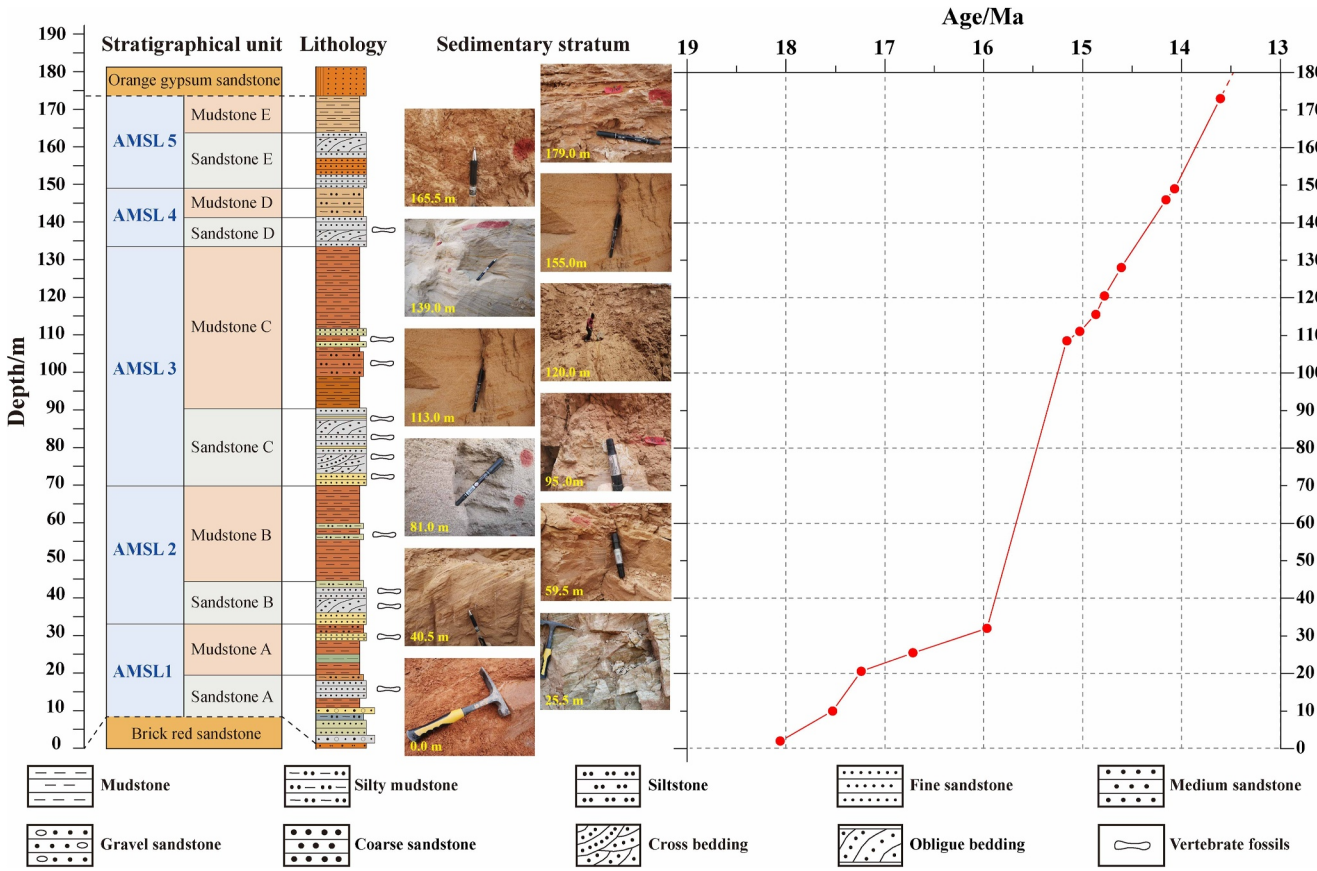

Figure 3. Depositional characteristic of the HJS stratigraphic outcrops in the field and a depth-age model based on linear interpolation. The dots represent the precise timing of geomagnetic polarity shifts as defined in GPTS2020 chronology.

correspond to C5Bn.1n and C5Bn.2n. Similarly, N3 and N2 are comparable to C5ADn and C5ACn, respectively, and the uppermost part of N1 is placed in the top red gypsum sandstone of unconstrained age.

Based on the comparison scheme described above, an age-depth linear interpolation method was employed to establish a chronological framework for the HJS section (Text S3 in Supporting Information S1; Figures S5–S7 in Supporting Information S1). By assuming uniform deposition rates within the same polarity period, ages corresponding to various depths can be obtained by interpolation. This analysis indicates that the age span of the entire sedimentary sequence, excluding the topmost 10 m, ranges from 18.2 to 13.5 Ma. Specifically, the lower portion of the Tongxin fauna (Yinziling Fauna) is dated to 18.0–15.9 Ma, while the upper portion (Ma'erzuiqigou Fauna) is approximately dated from 15.9 to 14.0 Ma. The sedimentation rate calculated from age-depth variation range is between ∼10 and ∼90 m/Ma, with an average of 30.68 m/Ma across the entire profile (Figure 3). These rates are comparable to those of other sections nearby Tongxin region (Liang et al., 2021; Wang et al., 2011; Wu et al., 2019; Zheng et al., 2023), affirming that our current comparison scheme aligns well with observed patterns of sedimentary evolution and regional geological context.

3.2. History of Vegetation and Climate Change in Tongxin Areas Across the MCO

The steppe biome predominated in the vicinity of the Tongxin Basin from 17.8 to 13.5 Ma. The dominant pollen types include the elements of boreal coniferous forest (e.g., *Pinus* and *Picea*), boreal broadleaved forest (e.g., *Betula* and *Quercus*), and herbs (e.g., Chenopodiaceae, *Artemisia*, Poaceae, Asteraceae), and the detailed pollen diagram is shown in Figure 4; Text S4 and Figures S8–S9 in Supporting Information S1. The percentage of tree pollen has a positive relationship with annual precipitation, particularly in arid and semi-arid areas, serving as a reliable proxy of effective moisture (Xiao et al., 2004; Zhao & Yu, 2012). Modern vegetation surveys and pollen-based reconstruction show that high values of tree pollen reflect a greater abundance of tree species favoring moist

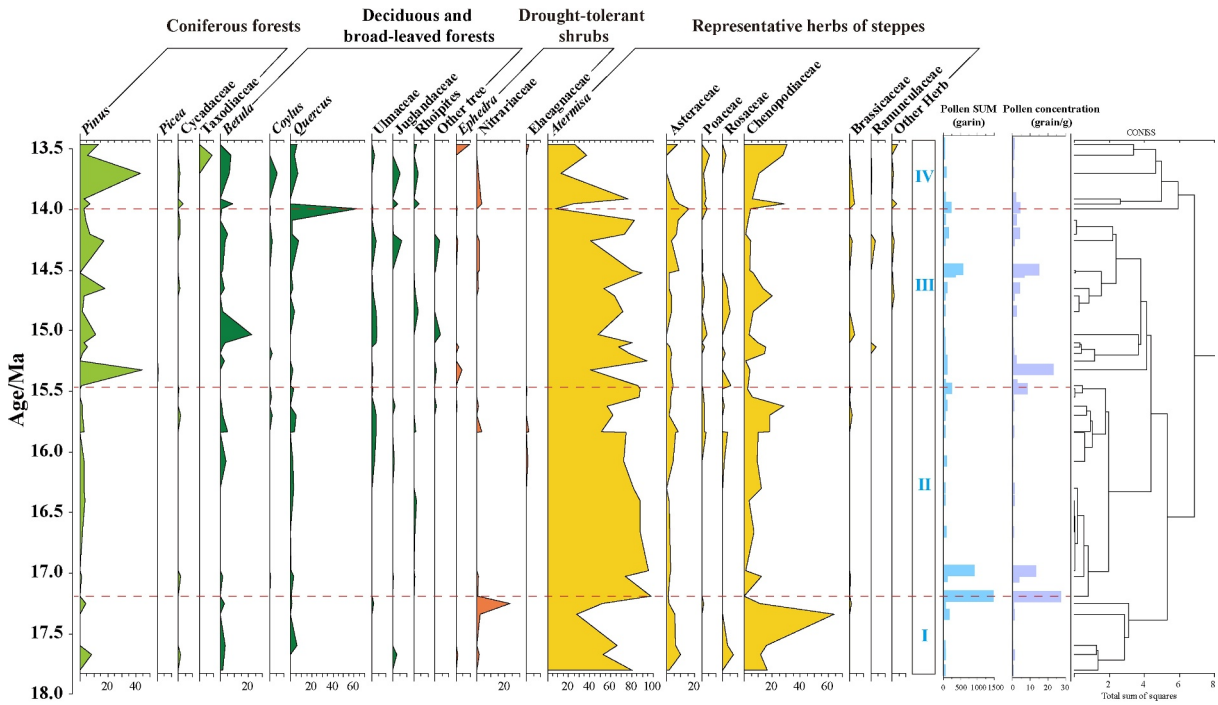

Figure 4. Pollen percentage diagram of major taxa from the HJS section. The pollen zonation is based on the CONISS result (Grimm, 1987), which shows the regional vegetation experienced four stages of transformation during 18.2–13.4 Ma.

conditions, notably deciduous and evergreen broadleaf forests, leading to a landscape predominantly covered by forests (Li et al., 2009). Some drought-resistant herbaceous plants, including species of *Artemisia*, Chenopodiaceae, Asteraceae, and *Ephedra*, will become dominant groups when the precipitation decreases to levels insufficient to support forest growth (Xu et al., 2005). Accordingly, HJS pollen data suggest that the study area experienced less precipitation during 17.8–16.0 Ma, supporting a vegetation landscape characterized by a relatively arid *Artemisia*-dominated steppe. Regional vegetation developed into relatively moist woodland steppe at 16.0–13.5 Ma with increasing precipitation, interspersed with mixed coniferous and broad-leaved forests during particularly humid intervals. In terms of variability, the regional vegetation pattern exhibits a transition from relatively stable to more rapid fluctuations during the middle MCO (Figure 5c).

Our high-resolution MS profile reflects those variations in MS values correlate well with changes in sedimentary facies (Figure 5d), underscoring the depositional environment as a primary factor influencing MS values. We primarily utilize this MS profile to assess the depositional environments alongside other proxy indicators. The coherent carbon-oxygen (C-O) isotope data are almost entirely distributed in fine-grained sediments, indicating that these isotopic signatures primarily represent shallow lake to floodplain environments, which implies sources of sediments were relatively stable. This is supported by fossil mammals and pollen data. In the subsequent interpretation of the significance of the isotope indications, we consider the influence of the depositional environment to be relatively constant.

The HJS $\delta^{13}C_{TOC}$ is likely to be indicative of regional temperature and C_4 plant ratio. Results show that $\delta^{13}C_{TOC}$ gradually drifts from −24‰ to −20.0‰ between 17.8 and 16.0 Ma, followed by a general increase and then a decrease during 16.0–14.2 Ma, which was accompanied by at least six rapid fluctuations ranging from −17.6‰ to −24.9‰ (Figure 5b). The pollen data show that no aquatic plants were detected throughout the entire sequence, and the terrestrial vegetation dominance implies the exogenous properties of the sediments. In any case, the fine-grained sediment in the profile originates from adjacent terrestrial deposits, and the ultimate TOC source therein is the overlying vegetation (Meyers & Ishiwatari, 1993). Previous studies have demonstrated that $\delta^{13}C_{TOC}$ is influenced by a combination of the relative proportion of C_3/C_4 plants and climatic factors. Calculation of C_4 biomass indicates the dominance of C_3 vegetation for most of the period except for the MCO (Text S5, Table S2 and Figure S11 in Supporting Information S1). Thus, in the MCO period, the HJS $\delta^{13}C_{TOC}$ values are influenced mainly

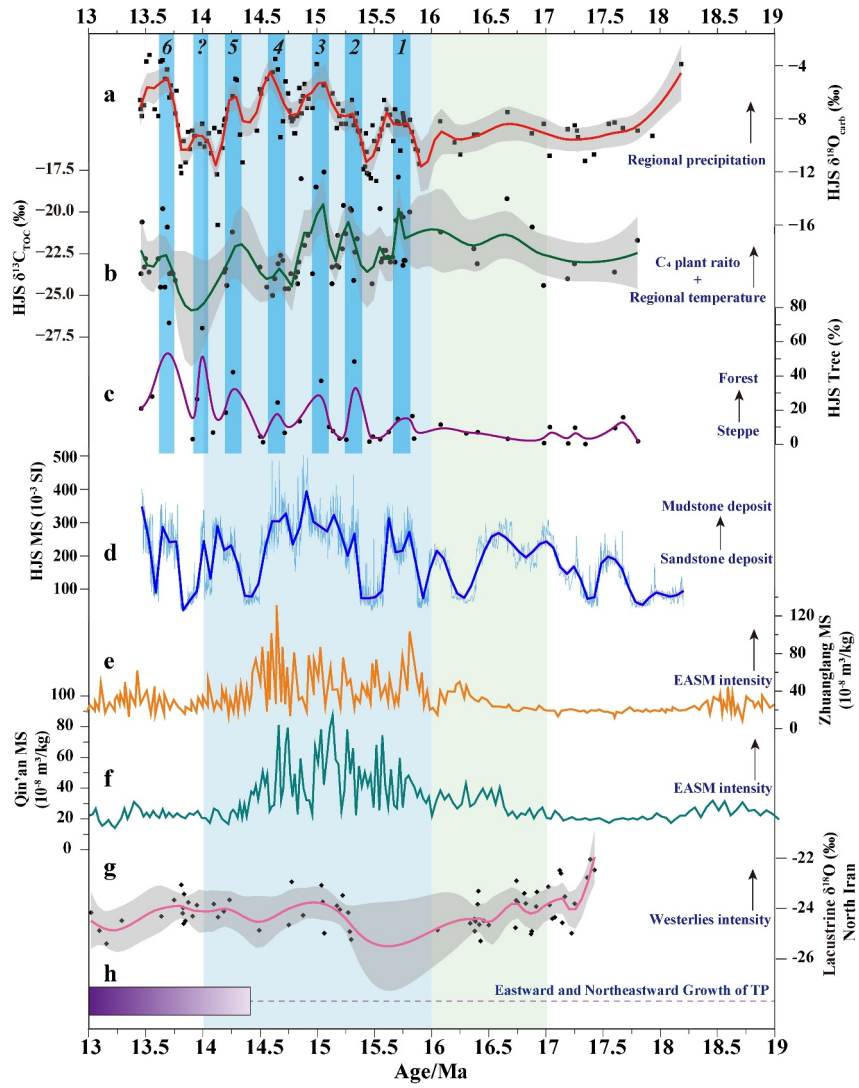

Figure 5. Comparison of vegetation-climate indices from the HJS section with other regional climate records during 19–13 Ma. The green and blue vertical shading corresponds to the early and late MCO. (a, b, d) $\delta^{18}O_{carb}$, $\delta^{13}C_{TOC}$ and magnetic susceptibility (MS) record of the HJS section (this study, these curves are subjected to LOESS (locally estimated scatterplot smoothing) smoothing and the bandwidths used as smoothing parameters were 0.1, 0.15, 0.05. Gray shading indicates 95% confidence intervals); (c) the percentage of the tree pollen (this study, soft curves show the distribution of peaks); (e–f) MS record from the Qin'an section (Guo et al., 2002) and Zhuanglang borehole (Dong et al., 2018); (g) Westerlies precipitation based on oxygen isotope data from North Iran (bandwidths=0.1) (Ballato et al., 2010). (h) The tectonic event of the third pulse of the Tibetan Plateau uplift starting at ~14.5 Ma (Clark et al., 2005; Wang et al., 2022).

by the $\delta^{13}C_{C3}$ value and C_4 plant ratio. Higher monsoon precipitation typically favors the growth of C_4 vegetation in water-limited regions (An et al., 2005; Sun et al., 2015; Yang et al., 2015), but also results in lower $\delta^{13}C_{TOC}$ values in C_3 plants (W. Liu et al., 2018). By contrast, warmer temperatures favor C_4 vegetation expansion and also increase $\delta^{13}C$ values of C_3 plants (Lu et al., 2017). Previous studies have shown that the mean $\delta^{13}C_{C3}$ value increases by 0.104‰ per 1°C temperature increase (Wang et al., 2013), and its control on the positive bias of plant carbon isotopes outweighs the inverse effects controlled by humidity and pCO_2 in North China (Lu et al., 2015). Meanwhile, since the minimum temperature during the growing season is an important limit for C_4 plants, temperature plays a critical role at mid-high latitudes (Zhang et al., 2003). Given the rain-heat synchronization of monsoon precipitation, we therefore consider temperature-dominated climatic factors and the proportion of C_4 vegetation to be the most critical determinants of $\delta^{13}C_{TOC}$. This is supported by the high correlation between the underlying pattern of the HJS $\delta^{13}C_{TOC}$ record and the global $\delta^{18}O$ data (relative temperature) across the MCO.

The HJS $\delta^{18}O_{carb}$ variations are tied to EASM precipitation intensity. The $\delta^{18}O_{carb}$ values were lower and stable during 18.0–16.0 Ma, while they increased and then decreased at 16.0–13.8 Ma interspersed with six rapid fluctuations (Figure 5a). Low $\delta^{13}C_{carb}$-$\delta^{18}O_{carb}$ correlation ($R^2 = 0.41$) indicates a more open water-influenced sedimentary system (Leng & Marshall, 2004; Li & Ku, 1997) (Figure S11 in Supporting Information S1), implying that authigenic carbonate $\delta^{18}O$ composition depends on $\delta^{18}O_{water}$ and water temperature. Given the $\delta^{18}O_{carb}$ is weakly controlled by water temperature (−0.26‰/1°C) and inconsistent with the global temperature record (Kele et al., 2015; Talbot, 1990), we argue that the HJS $\delta^{18}O_{carb}$ record mainly reflects changes in $\delta^{18}O_{atop\text{-}water}$ originating from regional precipitation. Comparison of modern monthly $\delta^{18}O_{atop\text{-}water}$ with climatic factors at nearby study sites (https://www.iaea.org/services/networks/gnip, Text S6, Figure S12 in Supporting Information S1), as well as geologic evidence (Gu, 1991; Han et al., 1997), suggests that $\delta^{18}O_{atop\text{-}water}$ is positively correlated with EASM intensity, which is generally associated with both warmer temperatures and increased summer rainfall in North China (Cheng et al., 2021). The six $\delta^{18}O_{carb}$ peaks in the late MCO are temporally synchronized with the high moisture index indicated by pollen evidence, which likely implies that the biased positive $\delta^{18}O_{carb}$ is indicative of an enhanced EASM.

3.3. Two-Stage Vegetation-Climate Response of the EASM Margin to the MCO

The analysis of diverse vegetation and climate indicators from the HJS section delineates a clear two-stage pattern during the MCO. This observation emerges from examining data variability and the alignment of principal peaks among various indicators, revealing consistent and comparable trends in multiple records. In the early MCO (∼17–∼16 Ma), indicators represented by pollen data exhibit low variability, suggesting the prevalence of a stable, arid steppe ecosystem within a warm-dry climatic setting. Conversely, the late MCO (∼16–∼14 Ma) is characterized by a significant increase in the variability of these indicators, marked by multiple fluctuations. More significantly, the peaks of the indicators have a good correspondence, which likely suggests that the vegetation and climate system of the Tongxin region in the late MCO were controlled by a unified driving factor. Based on the above comparisons and analyses, we tentatively propose a two-phase model for interpreting the changes in the regional vegetation-climate during the warm MCO.

To address potential influences arising from variations in sampling densities of the indicators across the two stages, we validated the HJS $\delta^{18}O_{carb}$ record as an example using both reduced data densities and interpolation-based time series analyses (Text S7 in Supporting Information S1). Comparison of the results before and after the reduction in data density shows that, despite a reduction in the clarity of several oscillations during the late MCO due to lower resolution, the two-phase model still holds in terms of variability indicated by the standard deviation (Figure S13 in Supporting Information S1). In addition, examination of the $\delta^{18}O_{carb}$ record for the ∼400-kyr periodicity reveals a distinct two-stage pattern throughout the MCO (Figure S14 in Supporting Information S1). Given the proposed two-stage model relies on data variability, we contend that the current sampling density has not substantial impact on the robustness of this model.

The sensitive response of plant communities in the region of the monsoon margin to warming during the MCO may explain the two-stage pattern of variability at Tongxin. The modern precipitation range in the Tongxin Basin is close to the threshold for forest growth, and the reconstruction shows a much wider range of variability in the EASM intensity during the MCO (Dong et al., 2018; Miao et al., 2023). Certain periods of high precipitation satisfy the threshold for woodland growth, and thus fluctuations in EASM intensity could be manifested as a rapid transition between the two ecotypes (forest-steppe). Integration of various indicators demonstrated that the early MCO period was characterized by gradual warming but low EASM precipitation, with strong evapotranspiration resulting in vegetation dominated by warm-dry steppe. By contrast, the late MCO period saw a significant increase in EASM intensity and instability under sustained warming. Despite the persistence of open steppe, stable forested environments emerged during periods of strong EASM, likely attributed to precipitation levels surpassing thresholds conducive to forest growth and diminished evaporation rates. Therefore, the vegetation landscape during this period showed a structure of multiple significant oscillatory changes.

Regional records support the prevalence of a two-stage pattern of change in EASM intensity. For example, two sets of robust age-controlled, high-resolution aeolian records (Zhuanglang and Qin'an) both show that the EASM intensity is persistently low in the early MCO (Guo et al., 2002; Qiang et al., 2010) (Figures 5e and 5f), whereas it is overall enhanced and fluctuates rapidly in the late MCO. The MS data from these two records indicate a nearly

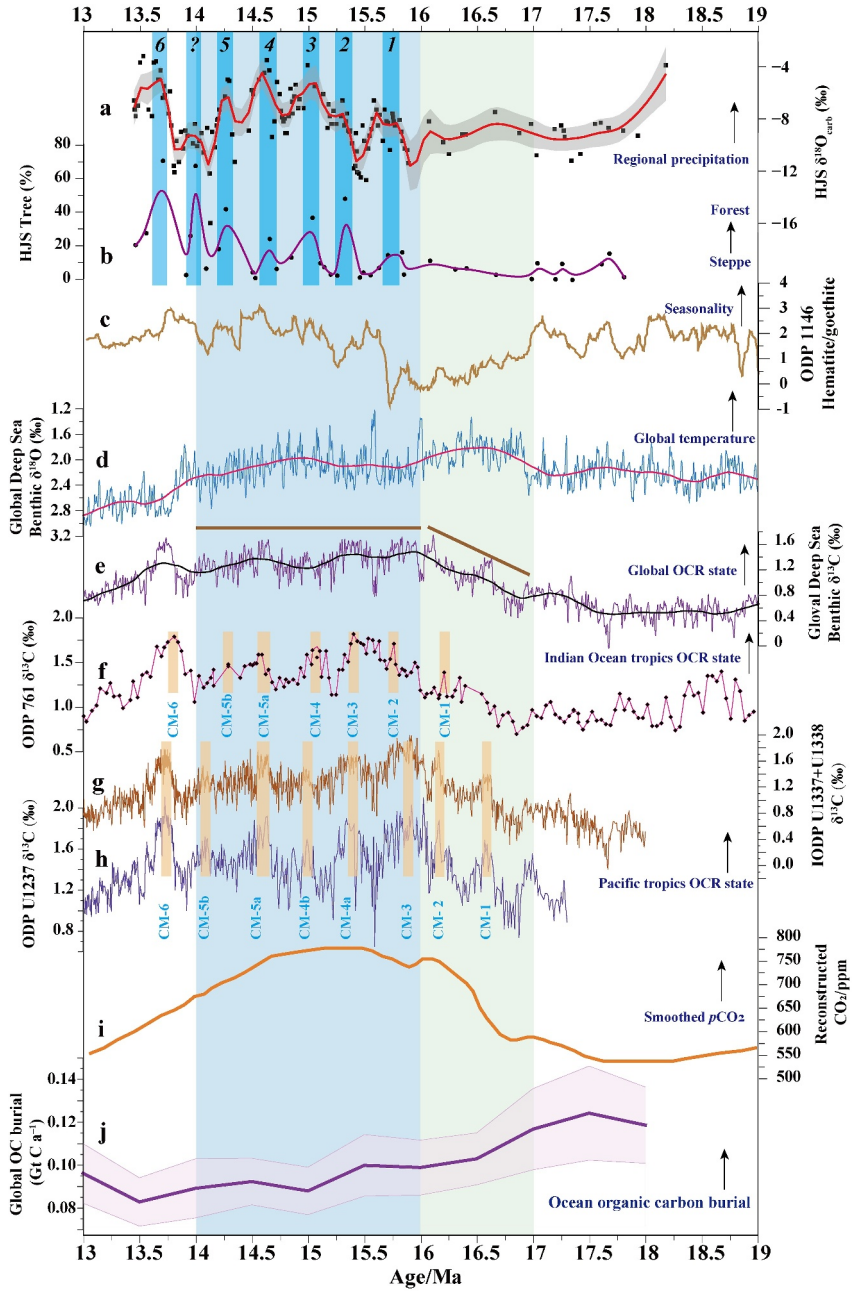

Figure 6. Comparison of vegetation-climate indices from the HJS section with marine records and reconstructed CO_2 during 19–13 Ma. The green and blue vertical shading corresponds to the early and late MCO. Cyan bands indicate peaks in multi-indicators and yellow bar represents the CM event. (a) $\delta^{18}O_{carb}$ record of the HJS section (this study); (b) the percentage of the tree pollen (this study); (c) Seasonality indicated by hematite/goethite ratio at ODP 1146 site in South China Sea (Clift, 2006); (d–e) Global benthic $\delta^{18}O$-$\delta^{13}C$ record (Westerhold et al., 2020); (f) Benthic $\delta^{13}C$ record and corresponding CM event form ODP 761 in the Indian Ocean tropics (Holbourn et al., 2004). (g–h) Benthic $\delta^{13}C$ record and corresponding CM event form IODP U1337 + U1338 and ODP U1237 site in the Pacific tropics (Holbourn et al., 2022). (i) The reconstructed atmospheric CO_2 curve after LOESS smoothing (Li et al., 2023). The raw data is based on marine proxies, including alkenones and boron methods (Rae et al., 2021). (j) Neogene organic carbon burial in the global ocean with ±1σ uncertainty envelope (Li et al., 2023).

synchronous and abrupt increase in the variability of the EASM intensity around ~16 Ma (Figure S15 in Supporting Information S1). This mode during the MCO is generally similar to our records, suggesting large-scale monsoon circulation is the dominant control over the regional environment. Therefore, we suggest that the

steady versus fluctuating pattern across the MCO stems from the coupling between the regional nature of the EASM system and the high sensitivity of vegetation at the monsoon margins, which contrasts with the global temperature pattern that rises and then falls (Figure 6d). At the end of the MCO, the reconstructed westerlies enhanced (Figure 5g) (Ballato et al., 2010), and the third uplift of the Tibetan Plateau in the late Middle Miocene had an increasingly significant impact on regional climate (Figure 5h) (Wang et al., 2022). We attribute the spatial differences in records near our study region to the combined influence of plateau uplift and changes in the westerlies, consistent with broader regional record integration results (Miao et al., 2012). This spatial heterogeneity in wetness also indicates that the EASM is no longer the decisive factor influencing regional precipitation after the MCO. Therefore, our discussion of the two-phase model is limited to the MCO.

3.4. Vegetation Ecosystem Oscillations Linked to OCR Perturbation in Late MCO

The most notable feature of the two-stage model is the onset of increased instability of the vegetation system at the mid-MCO. In the early MCO, regional temperature responded to global warming but arid steppe dominated, possibly indicating that warming-induced increases in monsoon precipitation failed to trigger conditions for woodland growth or that early MCO warming failed to increase EASM precipitation. The strong seasonality revealed by the South China Sea record from about 16 Ma onwards is likely to signal a stronger influence of the monsoon system on inland precipitation (Clift, 2006) (Figure 6c). Due to the evolution of the East Asian monsoon circulation coupling different Earth subsystems and being influenced by tectonic-interannual scale factors (Sun et al., 2022; Wang et al., 2017), it is particularly important to explore the main controlling factors and possible dynamic mechanisms of the two-phase model.

The multiple oscillations in the late MCO indicate a heightened influence of orbital-scale factors. Tectonic influences typically affect climate on million-year timescales in a unidirectional and irreversible manner (An et al., 2001; Molnar et al., 2010; Tada et al., 2016). We examined the sedimentary sequences in the HJS section corresponding to the MCO period and confirmed that there is no significant stratigraphic deformation or angular unconformity. Additionally, the reconstruction of the tectonic history of the Tongxin Basin further supported the tectonic stability of the area (Liang et al., 2021). Therefore, in our study, the tectonic stability provides a consistent baseline, allowing our records to more clearly detect orbital-scale climate signals. While we acknowledge the possibility of tectonic influences, it is evident that tectonic effects are not the decisive factor affecting the multiple oscillations during the late MCO in this study. Global mean temperatures reached their highest levels of the Neogene between 17 and 16 Ma (Auderset et al., 2022), yet a simple temperature control does not align with the stronger monsoon systems in the late MCO. While solar radiation plays an important role, its average levels during the MCO were generally uniform (Laskar et al., 2004), and its periodicity cannot explain the phase change characteristics. Therefore, it is likely that certain unclear nonlinear amplification effects highlight changes caused by other forcings (Burls et al., 2021). As part of the carbon cycle linking the ocean-atmosphere-monsoon system, CO_2 is likely a significant factor (Greenop et al., 2014). However, due to the lack of high-resolution, reliable reconstruction records (Consortium et al., 2023; Foster et al., 2012; Kürschner et al., 2008; Rae et al., 2021), its exact role is difficult to determine accurately.

OCR in the context of this warm period, served as a key linking hub in the context of this warm period (Holbourn et al., 2022; Sosdian & Lear, 2020), was more pronounced when the Antarctic ice-sheet was underdeveloped. Through the compilation of global, Pacific and Indian Ocean deep-sea records, we observed a continuous increase in benthic foraminiferal $\delta^{13}C$ values during 17.5–16.0 Ma, followed by sustained high values until 13.7 Ma (Holbourn et al., 2004; Tian et al., 2014; Westerhold et al., 2020) (Figures 6f–6h). In contrast, global temperatures exhibited a continuous decrease since 15 Ma in long-term trend, with only 2/3 of the Pleistocene climate impact (Holbourn et al., 2013; Lisiecki & Raymo, 2005). The seesaw shift between active OCR and attenuated temperatures likely suggests that the former acted as a greater nexus forcing during the late MCO. Previous studies demonstrated that the OCR was perturbed cyclically in the late MCO and its amplitude and frequency increased in the equatorial Pacific (Kochhann et al., 2016; Tian et al., 2013). Its signal of instability was manifested by several $\delta^{13}C_{max}$ (~400 ky period) events that occurred in the OCR perturbation during the mid-late MCO.

Further analysis of terrestrial and marine records supports a closer link between the EASM circulation system and the OCR during the mid-MCO. Through time-series analyses of representative indicators, we sought to elucidate the connection between the OCR and vegetation-climate dynamics at the monsoon margins. Periodic analyses

unveiled a significant ~400 kyr periodicity in both the HJS $\delta^{18}O_{carb}$ and MS data (Figure S16 in Supporting Information S1). This periodicity is also evident in the Zhuanglang borehole MS and marine ODP 761 benthic $\delta^{13}C$ record (Figure S17 in Supporting Information S1). Wavelet coherence analysis further demonstrates a clear positive correlation for the ~400 kyr periodicity between the HJS $\delta^{18}O_{carb}$ and ODP 761 $\delta^{13}C$ data, and IODP U1337 + U1338 benthic $\delta^{13}C$ data starting from 16 Ma (Figures 7a and 7b), providing robust support to our two-stage model for the MCO. Furthermore, wavelet analysis of the Zhuanglang borehole MS data alongside the ODP 761 $\delta^{13}C$ record corroborates a significant linkage between EASM precipitation and the marine carbon cycle on ~400 kyr periodicity (Figure 7c).

The multiple oscillations in EASM precipitation during the mid-late MCO are likely responding to feedback effects caused by strong perturbations in the OCR marked by C_{max} event, in addition to temperature control. Our preliminary examination shows that the occurrence of C_{max} event is slightly earlier or synchronous with changes in the terrestrial indicators at monsoon margins in most peak comparisons. This temporal precedence is reinforced by recent findings (F. Liu et al., 2024), which demonstrated that $\delta^{13}C$ (marine carbon cycle) leads $\delta^{18}O$ (climate-cryosphere system) on a 405 kyr timescale during the MCO. This lead-lag relationship is interpreted as an influx of external carbon sources associated with large emissions from flood basalt and tectonic degassing during the MCO (Herbert et al., 2022; Kasbohm & Schoene, 2018), amplifying the tropical hydrological cycle and accelerating the sensitivity of the low-latitude OCR's response to eccentricity forcing (F. Liu et al., 2024). Rising CO_2 concentrations lead to a significant increase in low-latitude tropical ocean temperatures and enrichment of the OCR with ^{13}C (Figure 6i), which seems to contradict the traditional belief that a stronger monsoon corresponds to more negative $\delta^{13}C$ values.

We propose a relatively reasonable and feasible explanation related to organic matter burial, although the intrinsic relationship between the C_{max} event and the monsoon system remains unclear. Recent studies have found that the enhanced temperature-dependent bacterial degradation leads to lower organic carbon (OC) burial rates during warmer periods (Li et al., 2023), resulting in more positive $\delta^{13}C$ values in the OCR. The degradation of large amounts of marine microorganisms releases significant CO_2 (John et al., 2014; Olivarez Lyle & Lyle, 2006), which can directly or indirectly enhance the monsoon system. This means that with the continuous increase in mid-low latitude ocean temperature, supported by global temperature reconstructions at different latitudes since 20 Ma showing a nearly 3°C increase in mid-low latitude ocean temperatures during the middle MCO (Herbert et al., 2022), CO_2 released by marine microbial activity acts as an additional forcing factor influencing the global carbon cycle and monsoon system. Theoretical calculations show lower marine organic matter burial in the late MCO (Figure 6j), supporting the notion that the impact of the oceanic carbon reservoir on the monsoon system cannot be ignored under sustained warm conditions (Li et al., 2023). The C_{max} event corresponds to lower organic matter burial rates, indicating a more profound influence of the OCR on the monsoon system during the mid-late MCO. Previous studies also show that the C_{max} event corresponds to highly unstable climate conditions (Wang et al., 2014), which can explain the significant oscillations in monsoon precipitation. Additionally, a warmer tropical ocean environment, corresponding to higher sea surface temperature (SST) or mean thermocline temperature anomaly (Dang et al., 2020; Fan et al., 2013), leads to a significant enhancement of the entire tropical hydrological cycle (Brook & Buizert, 2018). Simultaneously, enhanced insolation causes the Intertropical Convergence Zone (ITCZ) to shift northwards (Geen et al., 2020; Schneider et al., 2014), increasing the reach and intensity of the EASM. The intensification of these two low-latitude processes contributes to stronger monsoon dynamics and more precipitation. In other words, because the oceanic OC cycle acted as a positive feedback mechanism during past global warming events, the enhanced and multiple oscillations of the monsoon were observed in the late MCO.

Changes in the vegetation of the inland ecotone amplify the signal of OCR-influenced oscillations in EASM precipitation (Figure 8). We suggest that with the continued increase in temperature, CO_2 from the OCR has a more significant impact on the monsoon. This likely caused the EASM precipitation belt to advance in pulses into the forest-steppe transition zone, starting in the mid-MCO. During certain periods, higher summer precipitation facilitated the attainment of the minimum threshold (~400 mm) for forest growth in semi-arid regions (Wang, Pan, et al., 2020). This is supported by the rainfall reconstruction indicating approximately 600 mm of precipitation in the Tianshui Basin, located 260 km south of the study site (Hui et al., 2021). In contrast, the reduced precipitation during the other periods of the late MCO allowed the region to continue maintaining the dominance of an open steppe landscape. It is the amplification effect caused by geographic boundaries and humidity thresholds that ultimately leads to multiple alternations between woodland and steppe environments.

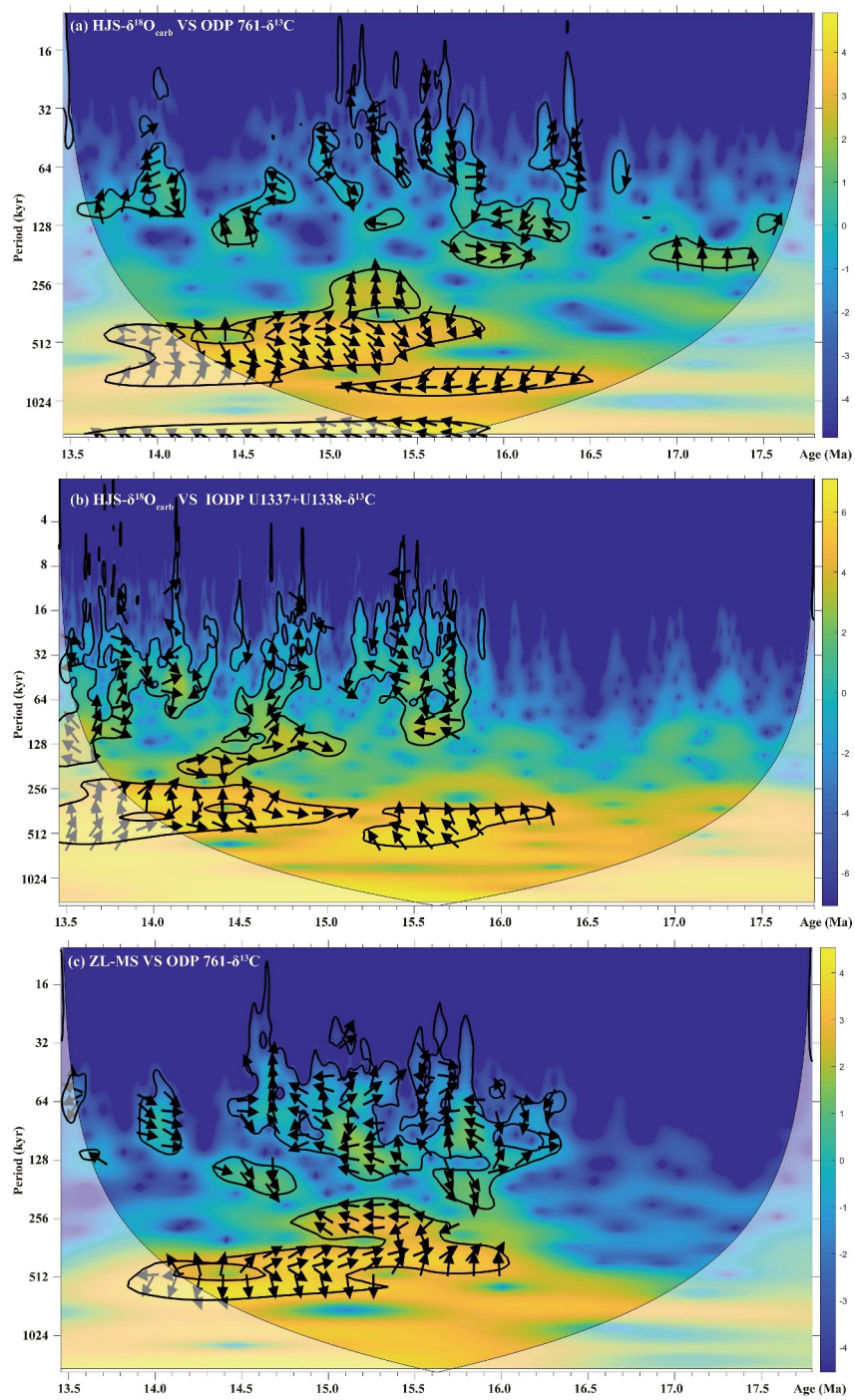

Figure 7. Wavelet and coherency analyses of study site record with regional and marine records. (a) $\delta^{18}O_{carb}$ of the HJS section indicative of precipitation variability in the Tongxin region with ODP 761 benthic $\delta^{13}C$ record reflecting the OCR state; (b) $\delta^{18}O_{carb}$ of the HJS section with IODP U1337 + U1338 benthic $\delta^{13}C$ record; (c) magnetic susceptibility record of the adjacent Zhuanglang borehole indicative of the East Asian summer monsoon strength with ODP761 benthic $\delta^{13}C$ record.

3.5. Insights From Comparisons With Middle Miocene Simulation Studies

Placing our research within the context of simulations allows for a better understanding of the dynamics of ocean-land connections during the MCO warming period. Our preliminary comparisons indicate that the latest simulation studies of the mid-Miocene generally support the EASM behavior observed in our data. We identify two

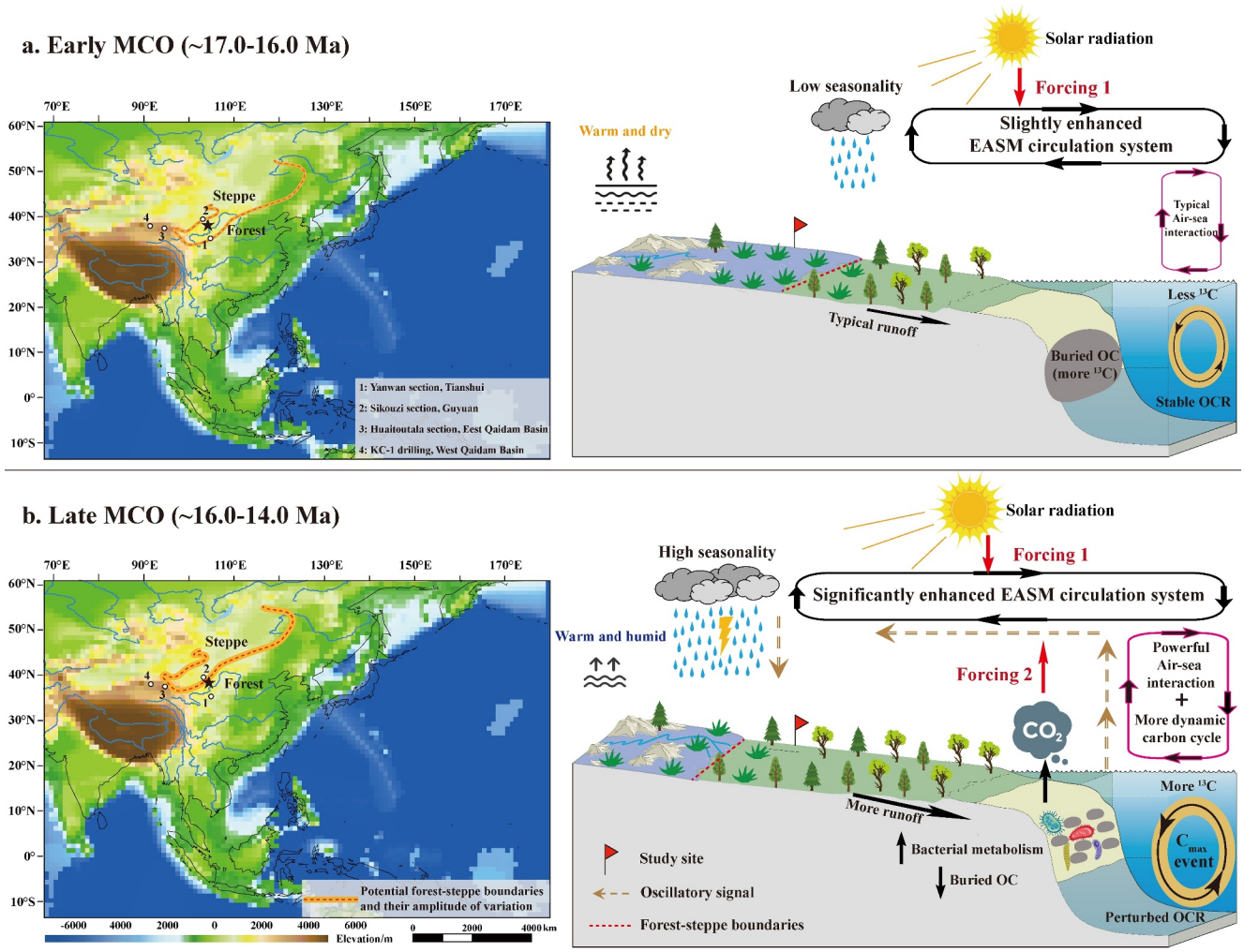

Figure 8. Schematic illustration of the OCR regulating the movement of forest-steppe boundaries via the East Asian summer monsoon in the early (a) and late (b) MCO. Base map based on Middle Miocene paleogeographic reconstructions (He et al., 2021). The potential boundary is inferred by the MCO pollen site and our published data set (Hui et al., 2011; Jiang & Ding, 2008; Miao et al., 2011, 2022; Wang et al., 2023), with analogy to the parallel movement of the modern boundary northwestward under equivalent warming scenarios.

primary driving processes from previous simulation studies that could be responsible for the evolution of the EASM circulation during the MCO. First, global warming enhanced the strength of the tropical hydrological cycle. The intensity of the global average hydrological cycle has been attributed to surface warming, with hydrological sensitivity increasing by 2.06% K^{-1} per degree of temperature rise (Held & Soden, 2006). Notably, the early-to-middle Miocene (E2MMIO) simulation found that with pCO_2 level ranging from 200 to 850 ppm, rainfall increases over much of northern Eurasia and the western Pacific warm pool (Krapp & Jungclaus, 2011), suggesting higher precipitation rates in the EASM region under warmer conditions (Acosta et al., 2023). Second, the greenhouse effect induced by high pCO_2 further strengthens the EASM circulation. Research indicates that an increase in pCO_2 from 280 to 400 ppm would result in a temperature rise of 2.9°C (Bradshaw et al., 2012). Elevated pCO_2 leads to higher global average temperatures, which in turn enhances global and regional precipitation rates and causes complex regional hydroclimate changes (Carmichael et al., 2016). In the E2MMIO model, increases in pCO_2 (400, 560, and 850 ppm) also support the intensification of regional hydrological cycles, with simulation-data consistency exceeding 80% in the Northern Hemisphere under high pCO_2 (Acosta et al., 2023). Specifically, for the EASM and ISM region, simulation results show that regional monthly

precipitation increases gradually as the pCO_2 rises (Douville et al., 2021; Geen et al., 2020), with this sensitivity being most pronounced in mid-high latitudes (Acosta et al., 2023). Given that pCO_2 fluctuated between ~280 and ~1,000 ppm during the MCO, with average concentrations being higher from 16 to 14 Ma than from 17 to 16 Ma (Burls et al., 2021; Steinthorsdottir, Coxall, et al., 2021), we suggest that a further strengthening of the EASM circulation in the late MCO is more reasonable. It is worth noting that recent studies indicate that an active AMOC under warm conditions promotes a southward shift in cross-equatorial atmospheric energy transport, thereby pushing the ITCZ northward (X. Liu et al., 2024). This process would likely affect the EASM, but the impact extent and spatiotemporal relationships await further exploration.

In contrast, the driving effects of paleogeography and ice sheets on EASM changes during the MCO were relatively limited. Previous estimates suggest that mid-Miocene topographic changes could only explain a 0.7°C warming (Krapp & Jungclaus, 2011). Additionally, the main ocean gateways remained stable during this period, and there was an absence of markable plateau uplift. Furthermore, tectonic events would interact with monsoons through physical barriers and the heat-driven air pump mechanism (Acosta & Huber, 2020; Boos & Kuang, 2010; Sarr et al., 2022; Wu et al., 2015), exhibiting complex regional differences and nonlinear responses. Thus, paleogeographic factors during this warm period can be considered a stable background, affecting monsoon behavior on million-year scales or during significant tectonic events (Farnsworth et al., 2019; Hu et al., 2023). Similarly, mid-Miocene ice sheets were limited in size and therefore had a minimal impact on tropical hydrological processes. However, some studies have suggested that the highly dynamic nature of the Antarctic ice sheet during the late MCO made it highly sensitive to orbital forcing (De Vleeschouwer et al., 2017; Miller et al., 2020), which bears some resemblance to the high variability in EASM behavior during the late MCO.

This preliminary comparison investigates the terrestrial environment's response to various forcings during the MCO from an Earth system science perspective. Our data show a correlation between stronger EASM circulation and warmer mid-to low-latitude oceans in the late MCO, a period marked by a reduced meridional temperature gradient. This supports the hypothesis that ocean heat content and the carbon cycle are likely decisive factors in controlling monsoon intensity (Jian et al., 2022). Current understanding of the detailed climate and environmental evolution during the MCO is still limited, some model-data inconsistencies may be related to state-dependent sensitivity, uncertainties in certain simulation parameters and the low resolution of proxies (Caballero & Huber, 2013). Nevertheless, improving data acquisition from crucial terrestrial regions and refining model-proxy comparisons will advance our understanding of the interactions between oceanic and terrestrial systems during the MCO. Integrating more terrestrial paleoclimate and paleovegetation data into simulations is crucial for clarifying hydroclimate evolution mechanisms during past warming periods.

4. Conclusions

We conducted a comprehensive study of the sedimentary sequence of the Tongxin Basin, located in the EASM margins. The results show that the vegetation and climate experienced two distinct stages across the MCO. They exhibit a pattern of flat stability in the early stage and intensified oscillations in the later stage. Combining the climatic significance of the different indicators, we conclude that regional vegetation is controlled by effective precipitation. Further comparison with reliable terrestrial and marine records attributes the cyclical changes in the late-stage forest and steppe environment to the rapid fluctuations in the EASM circulation system related to OCR oscillations.

Our results highlight the important role of low-latitude forcing on mid-latitude inland vegetation change in past warming periods. Despite the limitations of the current preliminary work in the quantitative reconstruction of vegetation patterns, it provides important data regarding changes in vegetation during the MCO. Significantly, in the context of warming, it sheds light on the need to consider the far-reaching impacts of the carbon cycle when considering climate environmental shifts in ecologically vulnerable inland areas.

Data Availability Statement

Our research data are available at (Wang, 2024). The data on which this article is based are available in (Wang, Deng, et al., 2016; Wang, Zong, et al., 2016).

Acknowledgments
We appreciate Xiaoke Qiang, Rancheng Xu, Jiacheng Ma, Wuyang Xiong, Haibin Wu, Yan Zhao and Zhuo Zheng for helpful suggestions and discussions; Liang Yu, Yong Yao, Liangqing Cheng, Zhipeng Wu, Mingsong Li and Yilun Yu for data analysis; Junnan Xu, Huihai Wang, and Zhongshen Wang for the pollen experiment. We gratefully acknowledge Editor-in-Chief Matthew Huber, the anonymous associate editor, Sarah Feakins, Tamara Fletcher and three anonymous reviewers for their constructive comments. Our work was supported by the National Program on Key Basic Research Project of China (2022YFF0801502, 2022YFF0801102), the National Natural Science Foundation of China (NSFC42303017, 41888101), the Fundamental Research Funds for the Central Universities (E3E40905), the Strategic Priority Research Program of Chinese Academy of Sciences (XDB26000000), and the Youth Innovation Promotion Association of the Chinese Academy of Sciences (2022071). The authors declare that they have no conflicts of interest regarding this work.

References

Acosta, R. P., Burls, N. J., Pound, M. J., Bradshaw, C. D., De Boer, A. M., Herold, N., et al. (2023). A model-data comparison of the hydrological response to Miocene Warmth: Leveraging the MioMIP1 opportunistic multi-model ensemble. *Paleoceanography and Paleoclimatology*, *39*(1), e2023PA004726. https://doi.org/10.1029/2023pa004726

Acosta, R. P., & Huber, M. (2020). Competing topographic mechanisms for the summer Indo-Asian monsoon. *Geophysical Research Letters*, *47*(3), e2019GL085112. https://doi.org/10.1029/2019gl085112

An, Z., Huang, Y., Liu, W., Guo, Z., Steven, C., Li, L., et al. (2005). Multiple expansions of C_4 plant biomass in East Asia since 7 Ma coupled with strengthened monsoon circulation. *Geology*, *33*(9), 705–708. https://doi.org/10.1130/g21423.1

An, Z., Kutzbach, J. E., Prell, W. L., & Porter, S. C. (2001). Evolution of Asian monsoons and phased uplift of the Himalaya-Tibetan plateau since Late Miocene times. *Nature*, *411*(6833), 62–66. https://doi.org/10.1038/35075035

Auderset, A., Moretti, S., Taphorn, B., Ebner, P. R., Kast, E., Wang, X. T., et al. (2022). Enhanced ocean oxygenation during Cenozoic warm periods. *Nature*, *609*(7925), 77–82. https://doi.org/10.1038/s41586-022-05017-0

Ballato, P., Mulch, A., Landgraf, A., Strecker, M. R., Dalconi, M. C., Friedrich, A., & Tabatabaei, S. H. (2010). Middle to late Miocene Middle Eastern climate from stable oxygen and carbon isotope data, southern Alborz mountains, N Iran. *Earth and Planetary Science Letters*, *300*(1–2), 125–138. https://doi.org/10.1016/j.epsl.2010.09.043

Boos, W. R., & Kuang, Z. (2010). Dominant control of the South Asian monsoon by orographic insulation versus plateau heating. *Nature*, *463*(7278), 218–222. https://doi.org/10.1038/nature08707

Bradshaw, C. D., Lunt, D. J., Flecker, R., Salzmann, U., Pound, M. J., Haywood, A. M., & Eronen, J. T. (2012). The relative roles of CO_2 and palaeogeography in determining late Miocene climate: Results from a terrestrial model–data comparison. *Climate of the Past*, *8*(4), 1257–1285. https://doi.org/10.5194/cp-8-1257-2012

Brook, E. J., & Buizert, C. (2018). Antarctic and global climate history viewed from ice cores. *Nature*, *558*(7709), 200–208. https://doi.org/10.1038/s41586-018-0172-5

Burls, N. J., Bradshaw, C. D., De Boer, A. M., Herold, N., Huber, M., Pound, M., et al. (2021). Simulating Miocene Warmth: Insights from an opportunistic multi-model ensemble (MioMIP1). *Paleoceanography and Paleoclimatology*, *36*(5), e2020PA004054. https://doi.org/10.1029/2020pa004054

Caballero, R., & Huber, M. (2013). State-dependent climate sensitivity in past warm climates and its implications for future climate projections. *Proceedings of the National Academy of Sciences of the United States of America*, *110*(35), 14162–14167. https://doi.org/10.1073/pnas.1303365110

Carmichael, M. J., Lunt, D. J., Huber, M., Heinemann, M., Kiehl, J., LeGrande, A., et al. (2016). A model–model and data–model comparison for the early Eocene hydrological cycle. *Climate of the Past*, *12*(2), 455–481. https://doi.org/10.5194/cp-12-455-2016

Chen, F., Chen, J., Huang, W., Chen, S., Huang, X., Jin, L., et al. (2019). Westerlies Asia and monsoonal Asia: Spatiotemporal differences in climate change and possible mechanisms on decadal to sub-orbital timescales. *Earth-Science Reviews*, *192*, 337–354. https://doi.org/10.1016/j.earscirev.2019.03.005

Cheng, H., Zhang, H., Cai, Y., Shi, Z., Yi, L., Deng, C., et al. (2021). Orbital-scale Asian summer monsoon variations: Paradox and exploration. *Science China Earth Sciences*, *64*(4), 529–544. https://doi.org/10.1007/s11430-020-9720-y

Clark, M. K., House, M. A., Royden, L. H., Whipple, K. X., Burchfiel, B. C., Zhang, X., & Tang, W. (2005). Late cenozoic uplift of southeastern Tibet. *Geology*, *33*(6), 525–528. https://doi.org/10.1130/g21265.1

Clift, P. D. (2006). Controls on the erosion of Cenozoic Asia and the flux of clastic sediment to the ocean. *Earth and Planetary Science Letters*, *241*(3–4), 571–580. https://doi.org/10.1016/j.epsl.2005.11.028

Consortium, C. C. P. I. P. C. P., Honisch, B., Royer, D. L., Breecker, D. O., Polissar, P. J., Bowen, G. J., et al. (2023). Toward a Cenozoic history of atmospheric CO(2). *Science*, *382*(6675), eadi5177. https://doi.org/10.1126/science.adi5177

Curio, J., Maussion, F., & Scherer, D. (2015). A 12-year high-resolution climatology of atmospheric water transport over the Tibetan Plateau. *Earth System Dynamics*, *6*(1), 109–124. https://doi.org/10.5194/esd-6-109-2015

Dang, H., Jian, Z., Wang, Y., Mohtadi, M., Rosenthal, Y., Ye, L., et al. (2020). Pacific warm pool subsurface heat sequestration modulated Walker circulation and ENSO activity during the Holocene. *Science Advances*, *6*(42). https://doi.org/10.1126/sciadv.abc0402

De Vleeschouwer, D., Vahlenkamp, M., Crucifix, M., & Pälike, H. (2017). Alternating Southern and Northern Hemisphere climate response to astronomical forcing during the past 35 m.y. *Geology*, *45*(4), 375–378. https://doi.org/10.1130/g38663.1

Diester-Haass, L., Billups, K., Jacquemin, I., Emeis, K. C., Lefebvre, V., & François, L. (2013). Paleoproductivity during the middle Miocene carbon isotope events: A data-model approach. *Paleoceanography*, *28*(2), 334–346. https://doi.org/10.1002/palo.20033

Ding, Y., & Chan, J. C. L. (2005). The East Asian summer monsoon: An overview. *Meteorology and Atmospheric Physics*, *89*(1–4), 117–142. https://doi.org/10.1007/s00703-005-0125-z

Dong, J., Liu, Z., An, Z., Liu, W., Zhou, W., Qiang, X., & Lu, F. (2018). Mid-Miocene C_4 expansion on the Chinese Loess Plateau under an enhanced Asian summer monsoon. *Journal of Asian Earth Sciences*, *158*, 153–159. https://doi.org/10.1016/j.jseaes.2018.02.014

Douville, H., Raghavan, K., Renwick, J., Allan, R. P., Arias, P. A., Barlow, M., et al. (2021). Water cycle changes. In V. P. Masson-Delmotte (Ed.), et al. (Eds.), *Climate change 2021: The physical science basis. Contribution of working group I to 45 the sixth assessment report of the intergovernmental panel on climate change* (pp. 1055–1210). Cambridge University Press. https://doi.org/10.1017/9781009157896.010x

Fan, L., Shin, S. I., Liu, Q., & Liu, Z. (2013). Relative importance of tropical SST anomalies in forcing East Asian summer monsoon circulation. *Geophysical Research Letters*, *40*(10), 2471–2477. https://doi.org/10.1002/grl.50494

Farnsworth, A., Lunt, D. J., Robinson, S. A., Valdes, P. J., Roberts, W. H. G., Clift, P. D., et al. (2019). Past East Asian monsoon evolution controlled by paleogeography, not CO_2. *Science Advances*, *5*(10), eaax1697. https://doi.org/10.1126/sciadv.aax1697

Foster, G. L., Lear, C. H., & Rae, J. W. B. (2012). The evolution of pCO_2, ice volume and climate during the middle Miocene. *Earth and Planetary Science Letters*, *341–344*, 243–254. https://doi.org/10.1016/j.epsl.2012.06.007

Geen, R., Bordoni, S., Battisti, D. S., & Hui, K. (2020). Monsoons, ITCZs, and the concept of the global monsoon. *Reviews of Geophysics*, *58*(4), e2020RG000700. https://doi.org/10.1029/2020rg000700

Greenop, R., Foster, G. L., Wilson, P. A., & Lear, C. H. (2014). Middle Miocene climate instability associated with high-amplitude CO_2 variability. *Paleoceanography*, *29*(9), 845–853. https://doi.org/10.1002/2014pa002653

Grimm, E. C. (1987). CONISS: A FORTRAN 77 program for stratigraphically constrained cluster analysis by the method of incremental sum of squares. *Computers & Geosciences*, *13*(1), 13–35. https://doi.org/10.1016/0098-3004(87)90022-7

Gu, Z. (1991). The carbonate isotopic composition of the loess-paleosol sequence and its implication of paleoclimatic change. *Chinese Science Bulletin*, *36*(23), 1979–1983. https://doi.org/10.1360/sb1991-36-23-1979

Guo, Z. T., Ruddiman, W. F., Hao, Q. Z., Wu, H. B., Qiao, Y. S., Zhu, R. X., et al. (2002). Onset of Asian desertification by 22 Myr ago inferred from loess deposits in China. *Nature*, *416*(6877), 159–163. https://doi.org/10.1038/416159a

Han, J., Keppens, E., Liu, T., Paepe, R., & Jiang, W. (1997). Stable isotope composition of the carbonate concretion in loess and climate change. *Quaternary International*, *37*, 37–43. https://doi.org/10.1016/1040-6182(96)00005-5

Harrison, T., Delson, E., & Jian, G. (1991). A new species of Pliopithecus from the middle Miocene of China and its implications for early catarrhine zoogeography. *Journal of Human Evolution*, *21*(5), 329–361. https://doi.org/10.1016/0047-2484(91)90112-9

He, Z., Zhang, Z., Guo, Z., Scotese, C. R., & Deng, C. (2021). Middle Miocene (~14 Ma) and late Miocene (~6 Ma) paleogeographic boundary conditions. *Paleoceanography and Paleoclimatology*, *36*(11), e2021PA004298. https://doi.org/10.1029/2021pa004298

Herbert, T. D., Dalton, C. A., Liu, Z., Salazar, A., Si, W., & Wilson, D. S. (2022). Tectonic degassing drove global temperature trends since 20 Ma. *Science*, *377*(6601), 116–119. https://doi.org/10.1126/science.abl4353

Holbourn, A., Kuhnt, W., Kochhann, K. G. D., Andersen, N., & Sebastian Meier, K. J. (2015). Global perturbation of the carbon cycle at the onset of the Miocene Climatic Optimum. *Geology*, *43*(2), 123–126. https://doi.org/10.1130/g36317.1

Holbourn, A., Kuhnt, W., Kochhann, K. G. D., Matsuzaki, K. M., & Andersen, N. (2022). Middle Miocene climate–carbon cycle dynamics: Keys for understanding future trends on a warmer Earth? In I. W. Aiello, J. A. Barron, & A. C. Ravelo (Eds.), *Understanding the monterey formation and similar biosiliceous units across space and time* (pp. 93–111). Geological Society of America. https://doi.org/10.1130/2022.2556(05

Holbourn, A., Kuhnt, W., Lyle, M., Schneider, L., Romero, O., & Andersen, N. (2013). Middle Miocene climate cooling linked to intensification of eastern equatorial Pacific upwelling. *Geology*, *42*(1), 19–22. https://doi.org/10.1130/g34890.1

Holbourn, A., Kuhnt, W., Simo, J. A., & Li, Q. (2004). Middle Miocene isotope stratigraphy and paleoceanographic evolution of the northwest and southwest Australian margins (Wombat Plateau and Great Australian Bight). *Palaeogeography, Palaeoclimatology, Palaeoecology*, *208*(1–2), 1–22. https://doi.org/10.1016/j.palaeo.2004.02.003

Hu, Y., Li, X., Boos, W. R., Guo, J., Lan, J., Lin, Q., et al. (2023). Emergence of the modern global monsoon from the Pangaea megamonsoon set by palaeogeography. *Nature Geoscience*, *16*(11), 1041–1046. https://doi.org/10.1038/s41561-023-01288-y

Hui, Z., Li, J., Xu, Q., Song, C., Zhang, J., Wu, F., & Zhao, Z. (2011). Miocene vegetation and climatic changes reconstructed from a sporopollen record of the Tianshui Basin, NE Tibetan Plateau. *Palaeogeography, Palaeoclimatology, Palaeoecology*, *308*(3–4), 373–382. https://doi.org/10.1016/j.palaeo.2011.05.043

Hui, Z., Zhou, X., Chevalier, M., Wei, X., Pan, Y., & Chen, Y. (2021). Miocene East Asia summer monsoon precipitation variability and its possible driving forces. *Palaeogeography, Palaeoclimatology, Palaeoecology*, *581*, 110609. https://doi.org/10.1016/j.palaeo.2021.110609

Jian, Z., Wang, Y., Dang, H., Mohtadi, M., Rosenthal, Y., Lea, D. W., et al. (2022). Warm pool ocean heat content regulates ocean-continent moisture transport. *Nature*, *612*(7938), 92–99. https://doi.org/10.1038/s41586-022-05302-y

Jiang, H., & Ding, Z. (2008). A 20 Ma pollen record of East-Asian summer monsoon evolution from Guyuan, Ningxia, China. *Palaeogeography, Palaeoclimatology, Palaeoecology*, *265*(1–2), 30–38. https://doi.org/10.1016/j.palaeo.2008.04.016

John, E. H., Wilson, J. D., Pearson, P. N., & Ridgwell, A. (2014). Temperature-dependent remineralization and carbon cycling in the warm Eocene oceans. *Palaeogeography, Palaeoclimatology, Palaeoecology*, *413*, 158–166. https://doi.org/10.1016/j.palaeo.2014.05.019

Kasbohm, J., & Schoene, B. (2018). Rapid eruption of the Columbia River flood basalt and correlation with the mid-Miocene climate optimum. *Science Advances*, *4*(9), eaat8223. https://doi.org/10.1126/sciadv.aat8223

Kele, S., Breitenbach, S. F. M., Capezzuoli, E., Meckler, A. N., Ziegler, M., Millan, I. M., et al. (2015). Temperature dependence of oxygen- and clumped isotope fractionation in carbonates: A study of travertines and tufas in the 6–95°C temperature range. *Geochimica et Cosmochimica Acta*, *168*, 172–192. https://doi.org/10.1016/j.gca.2015.06.032

Kochhann, K. G. D., Holbourn, A., Kuhnt, W., Channell, J. E. T., Lyle, M., Shackford, J. K., et al. (2016). Eccentricity pacing of eastern equatorial Pacific carbonate dissolution cycles during the Miocene Climatic Optimum. *Paleoceanography*, *31*(9), 1176–1192. https://doi.org/10.1002/2016pa002988

Krapp, M., & Jungclaus, J. H. (2011). The Middle Miocene climate as modelled in an atmosphere-ocean-biosphere model. *Climate of the Past*, *7*(4), 1169–1188. https://doi.org/10.5194/cp-7-1169-2011

Kürschner, W. M., Kvaček, Z., & Dilcher, D. L. (2008). The impact of Miocene atmospheric carbon dioxide fluctuations on climate and the evolution of terrestrial ecosystems. *Proceedings of the National Academy of Sciences of the United States of America*, *105*(2), 449–453. https://doi.org/10.1073/pnas.0708588105

Laskar, J., Robutel, P., Joutel, F., Gastineau, M., Correia, A. C. M., & Levrard, B. (2004). A long-term numerical solution for the insolation quantities of the Earth. *Astronomy & Astrophysics*, *428*(1), 261–285. https://doi.org/10.1051/0004-6361:20041335

Leng, M. J., & Marshall, J. D. (2004). Palaeoclimate interpretation of stable isotope data from lake sediment archives. *Quaternary Science Reviews*, *23*(7–8), 811–831. https://doi.org/10.1016/j.quascirev.2003.06.012

Li, C., Wang, S.-Q., & Yang, Q. (2022). Discovery of a primitive *Gomphotherium* from the Early Miocene of northern China and its biochronology and palaeobiogeography significance. *Historical Biology*, 1–9. https://doi.org/10.1080/08912963.2022.2077106

Li, H. C., & Ku, T. L. (1997). $\delta^{13}C$–$\delta^{18}C$ covariance as a paleohydrological indicator for closed-basin lakes. *Palaeogeography, Palaeoclimatology, Palaeoecology*, *133*(1–2), 69–80. https://doi.org/10.1016/s0031-0182(96)00153-8

Li, M., Hinnov, L., & Kump, L. (2019). Acycle: Time-series analysis software for paleoclimate research and education. *Computers & Geosciences*, *127*, 12–22. https://doi.org/10.1016/j.cageo.2019.02.011

Li, Y., Xu, Q., Zhang, L., Wang, X., Cao, X., & Yang, X. (2009). Modern pollen assemblages of the forest communities and their relationships with vegetation and climate in northern China. *Journal of Geographical Sciences*, *19*(6), 643–659. https://doi.org/10.1007/s11442-009-0643-6

Li, Z., Zhang, Y. G., Torres, M., & Mills, B. J. W. (2023). Neogene burial of organic carbon in the global ocean. *Nature*, *613*(7942), 90–95. https://doi.org/10.1038/s41586-022-05413-6

Liang, H., Zhang, K., Fu, J., Wang, W., Zhang, P., & Ma, Z. (2021). Sedimentary basin evolution and its implications for outward expansion of the northeastern Tibetan Plateau: Insights from the Tongxin Basin, China. *Palaeogeography, Palaeoclimatology, Palaeoecology*, *575*, 110460. https://doi.org/10.1016/j.palaeo.2021.110460

Lin, L., Hu, C., Wang, B., Wu, R., Wu, Z., Yang, S., et al. (2024). Atlantic origin of the increasing Asian westerly jet interannual variability. *Nature Communications*, *15*(1), 2155. https://doi.org/10.1038/s41467-024-46543-x

Lisiecki, L. E., & Raymo, M. E. (2005). A Pliocene-Pleistocene stack of 57 globally distributed benthic $\delta^{18}O$ records. *Paleoceanography*, *20*(1), PA1003. https://doi.org/10.1029/2004pa001071

Liu, F., Du, J., Huang, E., Ma, W., Ma, X., Lourens, L. J., & Tian, J. (2024). Accelerated marine carbon cycling forced by tectonic degassing over the Miocene Climate Optimum. *Science Bulletin*, *69*(6), 823–832. https://doi.org/10.1016/j.scib.2023.12.052

Liu, W., Li, X., Wang, Z., Wang, H., Liu, H., Zhang, B., & Zhang, H. (2018). Carbon isotope and environmental changes in lakes in arid Northwest China. *Science China Earth Sciences*, *62*(8), 1193–1206. https://doi.org/10.1007/s11430-018-9232-4

Liu, X., Hu, J., Shi, W., Chen, H., & Yan, J. (2019). Palaeogene–neogene sedimentary and tectonic evolution of the Yinchuan basin, western north China Craton. *International Geology Review*, *62*(1), 53–71. https://doi.org/10.1080/00206814.2019.1591309

Liu, X., Shi, W., Hu, J., Fu, J., Yan, J., & Sun, L. (2019). Magnetostratigraphy and tectonic implications of Paleogene-Neogene sediments in the Yinchuan Basin, western North China Craton. *Journal of Asian Earth Sciences*, *173*, 61–69. https://doi.org/10.1016/j.jseaes.2019.01.016

Lu, H., Zhang, H., Zeng, L., Lyu, A., Zhang, Z., Chen, Y., et al. (2015). Temperature forced vegetation varations in glacial interglacial cycles in northeastern China revealed by loess palesol deposit. *Quaternary Sciences*, *35*(4), 828–836. https://doi.org/10.11928/j.issn.1001-7410.2015.04.05

Lu, H., Zhou, Y., Liu, W., & Mason, J. (2017). Organic stable carbon isotopic composition reveals late Quaternary vegetation changes in the dune fields of northern China. *Quaternary Research*, *77*(3), 433–444. https://doi.org/10.1016/j.yqres.2012.01.009

Methner, K., Campani, M., Fiebig, J., Loffler, N., Kempf, O., & Mulch, A. (2020). Middle Miocene long-term continental temperature change in and out of pace with marine climate records. *Scientific Reports*, *10*(1), 7989. https://doi.org/10.1038/s41598-020-64743-5

Meyers, P. A., & Ishiwatari, R. (1993). Lacustrine organic geochemistry—An overview of indicators of organic matter sources and diagenesis in lake sediments. *Organic Geochemistry*, *20*(7), 867–900. https://doi.org/10.1016/0146-6380(93)90100-p

Miao, Y., Fang, X., Herrmann, M., Wu, F., Zhang, Y., & Liu, D. (2011). Miocene pollen record of KC-1 core in the Qaidam Basin, NE Tibetan Plateau and implications for evolution of the East Asian monsoon. *Palaeogeography, Palaeoclimatology, Palaeoecology*, *299*(1–2), 30–38. https://doi.org/10.1016/j.palaeo.2010.10.026

Miao, Y., Fang, X., Sun, J., Xiao, W., Yang, Y., Wang, X., et al. (2022). A new biologic paleoaltimetry indicating Late Miocene rapid uplift of northern Tibet Plateau. *Science*, *378*(6624), 1074–1079. https://doi.org/10.1126/science.abo2475

Miao, Y., Herrmann, M., Wu, F., Yan, X., & Yang, S. (2012). What controlled mid–late Miocene long-term aridification in Central Asia? — Global cooling or Tibetan plateau uplift: A review. *Earth-Science Reviews*, *112*(3–4), 155–172. https://doi.org/10.1016/j.earscirev.2012.02.003

Miao, Y., Zhang, T., Huang, K., Wang, X., Niu, G., Wang, X., et al. (2023). Pollen assemblages reflect a Mid-Miocene precipitation gradient in the northeastern Tibetan Plateau. *Palaeogeography, Palaeoclimatology, Palaeoecology*, *617*, 111514. https://doi.org/10.1016/j.palaeo.2023.111514

Miller, K. G., Browning, J. V., Schmelz, W. J., Kopp, R. E., Mountain, G. S., & Wright, J. D. (2020). Cenozoic sea-level and cryospheric evolution from deep-sea geochemical and continental margin records. *Science Advances*, *6*(20), eaaz1346. https://doi.org/10.1126/sciadv.aaz1346

Molnar, P., Boos, W. R., & Battisti, D. S. (2010). Orographic controls on climate and paleoclimate of Asia: Thermal and mechanical roles for the Tibetan plateau. *Annual Review of Earth and Planetary Sciences*, *38*(1), 77–102. https://doi.org/10.1146/annurev-earth-040809-152456

Ogg, J. G. (2020). Geomagnetic polarity time scale. In F. M. Gradstein, J. G. Ogg, M. D. Schmitz, & G. M. Ogg (Eds.), *Geologic time scale 2020* (pp. 159–192). Elsevier. https://doi.org/10.1016/b978-0-12-824360-2.00005-x

Olivarez Lyle, A., & Lyle, M. W. (2006). Missing organic carbon in Eocene marine sediments: Is metabolism the biological feedback that maintains end-member climates? *Paleoceanography*, *21*(2), PA2007. https://doi.org/10.1029/2005pa001230

Qiang, X., An, Z., Song, Y., Chang, H., Sun, Y., Liu, W., et al. (2010). New eolian red clay sequence on the western Chinese Loess Plateau linked to onset of Asian desertification about 25 Ma ago. *Science China Earth Sciences*, *54*(1), 136–144. https://doi.org/10.1007/s11430-010-4126-5

Qiu, Z., & Guan, J. (1986). A lower molar of Pliopithecus from Tongxin, Ningxia Hui Autonomous region. *Acta Anthropologica Sinica*, *5*(03), 201. https://www.anthropol.ac.cn/EN/Y1986/V5/I03/201

Rae, J. W. B., Zhang, Y. G., Liu, X., Foster, G. L., Stoll, H. M., & Whiteford, R. D. M. (2021). Atmospheric CO_2 over the past 66 million Years from marine archives. *Annual Review of Earth and Planetary Sciences*, *49*(1), 609–641. https://doi.org/10.1146/annurev-earth-082420-063026

Sarr, A.-C., Donnadieu, Y., Bolton, C. T., Ladant, J.-B., Licht, A., Fluteau, F., et al. (2022). Neogene South Asian monsoon rainfall and wind histories diverged due to topographic effects. *Nature Geoscience*, *15*(4), 314–319. https://doi.org/10.1038/s41561-022-00919-0

Schneider, T., Bischoff, T., & Haug, G. H. (2014). Migrations and dynamics of the intertropical convergence zone. *Nature*, *513*(7516), 45–53. https://doi.org/10.1038/nature13636

Shevenell, A. E., Kennett, J. P., & Lea, D. W. (2004). Middle Miocene southern ocean cooling and Antarctic cryosphere expansion. *Science*, *305*(5691), 1766–1770. https://doi.org/10.1126/science.1100061

Shi, W., Dong, S., Liu, Y., Hu, J., Chen, X., & Chen, P. (2015). Cenozoic tectonic evolution of the South Ningxia region, northeastern Tibetan Plateau inferred from new structural investigations and fault kinematic analyses. *Tectonophysics*, *649*, 139–164. https://doi.org/10.1016/j.tecto.2015.02.024

Sosdian, S. M., Babila, T. L., Greenop, R., Foster, G. L., & Lear, C. H. (2020). Ocean carbon storage across the middle Miocene: A new interpretation for the Monterey event. *Nature Communications*, *11*(1), 134. https://doi.org/10.1038/s41467-019-13792-0

Sosdian, S. M., & Lear, C. H. (2020). Initiation of the western Pacific warm pool at the middle Miocene climate transition? *Paleoceanography and Paleoclimatology*, *35*(12), e2020PA003920. https://doi.org/10.1029/2020pa003920

Steinthorsdottir, M., Coxall, H. K., de Boer, A. M., Huber, M., Barbolini, N., Bradshaw, C. D., et al. (2021). The Miocene: The future of the past. *Paleoceanography and Paleoclimatology*, *36*(4), e2020PA004037. https://doi.org/10.1029/2020pa004037

Steinthorsdottir, M., Jardine, P. E., & Rember, W. C. (2021). Near-future pCO_2 during the Hot Miocene climatic optimum. *Paleoceanography and Paleoclimatology*, *36*(1), e2020PA003900. https://doi.org/10.1029/2020pa003900

Su, Y., Guo, Q., Hu, T., Guan, H., Jin, S., An, S., et al. (2020). An updated vegetation map of China (1:1000000). *Science Bulletin*, *65*(13), 1125–1136. https://doi.org/10.1016/j.scib.2020.04.004

Sun, Y., Kutzbach, J., An, Z., Clemens, S., Liu, Z., Liu, W., et al. (2015). Astronomical and glacial forcing of East Asian summer monsoon variability. *Quaternary Science Reviews*, *115*, 132–142. https://doi.org/10.1016/j.quascirev.2015.03.009

Sun, Y., Wang, T., Yin, Q., Lyu, A., Crucifix, M., Cai, Y., et al. (2022). A review of orbital-scale monsoon variability and dynamics in East Asia during the Quaternary. *Quaternary Science Reviews*, *288*, 107593. https://doi.org/10.1016/j.quascirev.2022.107593

Tada, R., Zheng, H., & Clift, P. D. (2016). Evolution and variability of the Asian monsoon and its potential linkage with uplift of the Himalaya and Tibetan Plateau. *Progress in Earth and Planetary Science*, *3*(1), 1–26. https://doi.org/10.1186/s40645-016-0080-y

Talbot, M. R. (1990). A review of the palaeohydrological interpretation of carbon and oxygen isotopic ratios in primary lacustrine carbonates. *Chemical Geology: Isotope Geoscience section*, *80*(4), 261–279. https://doi.org/10.1016/0168-9622(90)90009-2

Tian, J., Ma, W., Lyle, M. W., & Shackford, J. K. (2014). Synchronous mid-Miocene upper and deep oceanic $\delta^{13}C$ changes in the east equatorial Pacific linked to ocean cooling and ice sheet expansion. *Earth and Planetary Science Letters*, *406*, 72–80. https://doi.org/10.1016/j.epsl.2014.09.013

Tian, J., Yang, M., Lyle, M. W., Wilkens, R., & Shackford, J. K. (2013). Obliquity and long eccentricity pacing of the Middle Miocene climate transition. *Geochemistry, Geophysics, Geosystems*, *14*(6), 1740–1755. https://doi.org/10.1002/ggge.20108

Wang, F., Pan, X., Gerlein-Safdi, C., Cao, X., Wang, S., Gu, L., et al. (2020). Vegetation restoration in northern China: A contrasted picture. *Land Degradation & Development*, *31*(6), 669–676. https://doi.org/10.1002/ldr.3314

Wang, G., Li, J., Liu, X., & Li, X. (2013). Variations in carbon isotope ratios of plants across a temperature gradient along the 400 mm isoline of mean annual precipitation in north China and their relevance to paleovegetation reconstruction. *Quaternary Science Reviews*, *63*, 83–90. https://doi.org/10.1016/j.quascirev.2012.12.004

Wang, J. (2024). Wang Jian-HJS-research data [Dataset]. *Figshare*. https://doi.org/10.6084/m9.figshare.25466656.v1

Wang, J., Zhou, X., Wang, S., Xu, H., Behling, H., Ye, J., et al. (2023). C_4 expansion of Central Asia in the middle Miocene linked to the strengthening Indian monsoon. *Global and Planetary Change*, *224*, 104096. https://doi.org/10.1016/j.gloplacha.2023.104096

Wang, P., Clemens, S., Tada, R., & Murray, R. (2019). Blowing in the monsoon wind. *Oceanography*, *32*(1), 48–59. https://doi.org/10.5670/oceanog.2019.119

Wang, P., Li, Q., Tian, J., Jian, Z., Liu, C., Li, L., & Ma, W. (2014). Long-term cycles in the carbon reservoir of the quaternary ocean: A perspective from the South China sea. *National Science Review*, *1*(1), 119–143. https://doi.org/10.1093/nsr/nwt028

Wang, P. X., Wang, B., Cheng, H., Fasullo, J., Guo, Z., Kiefer, T., & Liu, Z. (2017). The global monsoon across time scales: Mechanisms and outstanding issues. *Earth-Science Reviews*, *174*, 84–121. https://doi.org/10.1016/j.earscirev.2017.07.006

Wang, S., Deng, T., Ye, J., He, W., & Chen, S. (2016). Morphological and ecological diversity of Amebelodontidae (Proboscidea, Mammalia) revealed by a Miocene fossil accumulation of an upper-tuskless proboscidean. *Journal of Systematic Palaeontology*, *15*(8), 601–615. https://doi.org/10.1080/14772019.2016.1208687

Wang, S., Zong, L., Yang, Q., Sun, B., Li, Y., Shi, Q., et al. (2016). Biostratigraphic subdividing of the Neogene Dingjia'ergou mammalian fauna, Tongxin County, Ningxia Province, and its background for the uplift of the Tibetan plateau. *Quaternary Sciences*, *36*(4), 789–809. https://doi.org/10.11928/j.issn.1001-7410.2016.04.02

Wang, W., Zhang, P., Garzione, C. N., Liu, C., Zhang, Z., Pang, J., et al. (2022). Pulsed rise and growth of the Tibetan Plateau to its northern margin since ca. 30 Ma. *Proceedings of the National Academy of Sciences of the United States of America*, *119*(8), e2120364119. https://doi.org/10.1073/pnas.2120364119

Wang, W., Zhang, P., Kirby, E., Wang, L., Zhang, G., Zheng, D., & Chai, C. Z. (2011). A revised chronology for Tertiary sedimentation in the Sikouzi basin: Implications for the tectonic evolution of the northeastern corner of the Tibetan Plateau. *Tectonophysics*, *505*(1–4), 100–114. https://doi.org/10.1016/j.tecto.2011.04.006

Warny, S., Askin, R. A., Hannah, M. J., Mohr, B. A. R., Raine, J. I., Harwood, D. M., & Florindo, F. (2009). Palynomorphs from a sediment core reveal a sudden remarkably warm Antarctica during the middle Miocene. *Geology*, *37*(10), 955–958. https://doi.org/10.1130/g30139a.1

Westerhold, T., Marwan, N., Drury, A. J., Liebrand, D., Agnini, C., Anagnostou, E., et al. (2020). An astronomically dated record of Earth's climate and its predictability over the last 66 million years. *Science*, *369*(6509), 1383–1387. https://doi.org/10.1126/science.aba6853

Wu, G., Duan, A., Liu, Y., Mao, J., Ren, R., Bao, Q., et al. (2015). Tibetan plateau climate dynamics: Recent research progress and outlook. *National Science Review*, *2*(1), 100–116. https://doi.org/10.1093/nsr/nwu045

Wu, J., Guo, L., Xiong, S., Wang, S., Tang, Z., Jin, C., et al. (2019). New magnetic constraints on early-middle Miocene uplift of the Liupan Shan, northeastern margin of the Tibetan plateau. *Geochemistry, Geophysics, Geosystems*, *20*(3), 1340–1357. https://doi.org/10.1029/2018gc007944

Wubben, E., Veenstra, T., Witkowski, J., Raffi, I., Hilgen, F., Bos, R., et al. (2023). Astrochronology of the Miocene climatic optimum record from ocean Drilling program site 959 in the eastern equatorial Atlantic. *Newsletters on Stratigraphy*, *56*(4), 457–484. https://doi.org/10.1127/nos/2023/0749

Xiao, J., Xu, Q., Nakamura, T., Yang, X., Liang, W., & Inouchi, Y. (2004). Holocene vegetation variation in the Daihai lake region of north-central China: A direct indication of the Asian monsoon climatic history. *Quaternary Science Reviews*, *23*(14–15), 1669–1679. https://doi.org/10.1016/j.quascirev.2004.01.005

Xiong, W. (2022). New species of *Percrocuta* (Carnivora, Hyaenidae) from the early middle Miocene of Tongxin, China. *Historical Biology*, *35*(5), 799–820. https://doi.org/10.1080/08912963.2022.2067757

Xu, Q., Li, Y., Yang, X., & Deng, Z. (2005). Study on surface pollen of major steppe communities in northern China. *Geographical Research*, *24*(3), 394–402. https://doi.org/10.11821/yj2005030008

Yang, S., Ding, Z., Li, Y., Wang, X., Jiang, W., & Huang, X. (2015). Warming-induced northwestward migration of the East Asian monsoon rain belt from the Last Glacial Maximum to the mid-Holocene. *Proceedings of the National Academy of Sciences of the United States of America*, *112*(43), 13178–13183. https://doi.org/10.1073/pnas.1504688112

Zachos, J. C., Dickens, G. R., & Zeebe, R. E. (2008). An early Cenozoic perspective on greenhouse warming and carbon-cycle dynamics. *Nature*, *451*(7176), 279–283. https://doi.org/10.1038/nature06588

Zhang, Z., Zhao, M., Lu, H., & Faiia, A. M. (2003). Lower temperature as the main cause of C_4 plant declines during the glacial periods on the Chinese Loess Plateau. *Earth and Planetary Science Letters*, *214*(3–4), 467–481. https://doi.org/10.1016/s0012-821x(03)00387-x

Zhao, Y., Tzedakis, P. C., Li, Q., Qin, F., Cui, Q., Liang, C., et al. (2020). Evolution of vegetation and climate variability on the Tibetan Plateau over the past 1.74 million years. *Science Advances*, *6*(19), eaay6193. https://doi.org/10.1126/sciadv.aay6193

Zhao, Y., & Yu, Z. (2012). Vegetation response to Holocene climate change in East Asian monsoon-margin region. *Earth-Science Reviews*, *113*(1–2), 1–10. https://doi.org/10.1016/j.earscirev.2012.03.001

Zheng, Y., Qiu, Z., Qiu, Z., Li, L., Wei, X., Zhang, R., et al. (2023). Revised magnetostratigraphy of the Linxia Basin in the northeast Tibetan Plateau, constrained by micromammalian fossils. *Palaeogeography, Palaeoclimatology, Palaeoecology*, *623*, 111620. https://doi.org/10.1016/j.palaeo.2023.111620

Zhou, X., Yang, J., Xiao, G., Wang, J., Hu, Y., Zheng, Y., et al. (2023). Megacycles of climate and vegetation in east Asia since 3 Ma. *Catena*, *229*, 107195. https://doi.org/10.1016/j.catena.2023.107195

References From the Supporting Information

Bowen, G. J., & Wilkinson, B. (2002). Spatial distribution of $\delta^{18}O$ in meteoric precipitation. *Geology*, *30*(4), 315. https://doi.org/10.1130/0091-7613(2002)030<0315:Sdooim>2.0.Co;2

Brugnoli, E., & Farquhar, G. D. (2000). Photosynthetic fractionation of carbon isotopes. In R. C. Leegood, T. D. Sharkey, & S. vonCaemmerer (Eds.), *Photosynthesis: Physiology and Metabolism* (pp. 399–434). Springer. https://doi.org/10.1007/0-306-48137-5_17

Collister, J. W., Rieley, G., Stern, B., Eglinton, G., & Fry, B. (1994). Compound-specific $\delta^{13}C$ analyses of leaf lipids from plants with differing carbon dioxide metabolisms. *Organic Geochemistry*, *21*(6–7), 619–627. https://doi.org/10.1016/0146-6380(94)90008-6

Dong, X., Li, Z., Liu, X., Jing, X., Cui, J., Huang, T., et al. (2022). Eogene to Neogene north-eastward expansion of the arcuate tectonic belt in north-east Tibetan Plateau: Constraints from detrital zircon geochronology and heavy minerals. *Geological Journal*, *57*(9), 3601–3622. https://doi.org/10.1002/gj.4490

Farquhar, G. D., Ehleringer, J. R., & Hubick, K. T. (1989). Carbon isotope discrimination and photosynthesis. *Annual Review of Plant Biology*, *40*(1), 503–537. https://doi.org/10.1146/annurev.pp.40.060189.002443

Han, J., Jiang, W., & Liu, D. (1996). Carbonate isotopic records of paleoclimate changes in Chinese loess. *Science in China. Series D*, *39*, 460–467.

He, Y., Yan, H., Ma, L., Zhang, L., Qiu, L., & Yang, S. (2019). Spatiotemporal dynamics of the vegetation in Ningxia, China using MODIS imagery. *Frontiers of Earth Science*, *14*(1), 221–235. https://doi.org/10.1007/s11707-019-0767-7

Jiang, Z., Li, C., Wang, S., & Sun, D. (2019). *Amphicyon zhanxiangi*, sp. nov., a new amphicyonid (Mammalia, Carnivora) from northern China. *Journal of Vertebrate Paleontology*, *38*(6), e1539857. https://doi.org/10.1080/02724634.2018.1539857

Jones, C. H. (2002). User-driven integrated software lives: "Paleomag" paleomagnetics analysis on the Macintosh. *Computers & Geosciences*, *28*(10), 1145–1151. https://doi.org/10.1016/s0098-3004(02)00032-8

Kirschvink, J. L. (1980). The least-squares line and plane and the analysis of palaeomagnetic data. *Geophysical Journal International*, *62*(3), 699–718. https://doi.org/10.1111/j.1365-246X.1980.tb02601.x

Lease, R. O., Nie, J., Horton, B. K., & Hoke, G. D. (2014). Cenozoic mountain building on the northeastern Tibetan Plateau. In *Toward an improved understanding of uplift mechanisms and the elevation history of the Tibetan plateau*. Geological Society of America. https://doi.org/10.1130/2014.2507(06

Li, X., & Du, N. (1999). The acid-alkali-free analysis of Quaternary pollen. *Journal of Integrative Plant Biology*, *41*(7), 782–784.

Moore, P. D., Collinson, M. E., & Webb, J. (1991). *Pollen analysis*. Blackwell Scientific Publications.

Nordt, L. C., Boutton, T. W., Jacob, J. S., & Mandel, R. D. (2002). C_4 plant productivity and climate-CO_2 variations in south-central Texas during the late quaternary. *Quaternary Research*, *58*(2), 182–188. https://doi.org/10.1006/qres.2002.2344

Peppe, D. J., Cote, S. M., Deino, A. L., Fox, D. L., Kingston, J. D., Kinyanjui, R. N., et al. (2023). Oldest evidence of abundant C_4 grasses and habitat heterogeneity in eastern Africa. *Science*, *380*(6641), 173–177. https://doi.org/10.1126/science.abq2834

Quidelleur, X., Holt, J., & Valet, J.-P. (1995). Confounding influence of magnetic fabric on sedimentary records of a field reversal. *Nature*, *374*(6519), 246–249. https://doi.org/10.1038/374246a0

Tauxe, L. (2010). *Essentials of paleomagnetism*. University of California Press.

Wang, G., Feng, X., Han, J., Zhou, L., Tan, W., & Su, F. (2008). Paleovegetation reconstruction using $\delta^{13}C$ of soil organic matter. *Biogeosciences*, *5*(5), 1325–1337. https://doi.org/10.5194/bg-5-1325-2008

Wang, S. (2020). The anthracotheres from northern Junggar Basin and their palaeoclimatic significance in relation to the Tibetan Plateau. *Palaeobiodiversity and Palaeoenvironments*, *101*(3), 839–852. https://doi.org/10.1007/s12549-020-00441-4

Wang, W., Zhang, P., Wang, Z., Liu, K., Xu, H., Liu, C., et al. (2020). Multiproxy records in middle–late Miocene sediments from the Wushan Basin: Implications for climate change and tectonic deformation in the northeastern Tibetan Plateau. *GSA Bulletin*, *133*(1–2), 149–158. https://doi.org/10.1130/b35635.1

Wang, X., Tseng, Z., Wu, W., Ye, J., Meng, J., & Bi, S. (2020). A new species of *Tunguractis* Colbert, 1939 (Carnivora, Hyaenidae) from the middle Miocene of Junggar basin, northwestern China and the early divergence of basal hyaenids in East Asia. *Geodiversitas*, *42*(3), 29. https://doi.org/10.5252/geodiversitas2020v42a3

Wynn, J. G. (2007). Carbon isotope fractionation during decomposition of organic matter in soils and paleosols: Implications for paleoecological interpretations of paleosols. *Palaeogeography, Palaeoclimatology, Palaeoecology*, *251*(3–4), 437–448. https://doi.org/10.1016/j.palaeo.2007.04.009

Yuan, D. Y., Ge, W. P., Chen, Z. W., Li, C. Y., Wang, Z. C., Zhang, H. P., et al. (2013). The growth of northeastern Tibet and its relevance to large-scale continental geodynamics: A review of recent studies. *Tectonics*, *32*(5), 1358–1370. https://doi.org/10.1002/tect.20081

Zhang, H., Ait Brahim, Y., Li, H., Zhao, J., Kathayat, G., Tian, Y., et al. (2019). The Asian summer monsoon: Teleconnections and forcing mechanisms—A review from Chinese Speleothem $\delta^{18}O$ records. *Quaternary*, *2*(3), 26. https://doi.org/10.3390/quat2030026

Zijderveld, J. D. A. (1967). A. C. Demagnetization of Rocks: Analysis of results. In D. W. Collinson, K. M. Creer, & S. K. Runcorn (Eds.), *Developments in Solid Earth Geophysics*, (pp. 254–286). Elsevier. https://doi.org/10.1016/B978-1-4832-2894-5.50049-5